Title: Extreme glacial cooling likely led to hominin depopulation of Europe in the Early Pleistocene

Authors: Vasiliki Margari[1], David A. Hodell[2], Simon A. Parfitt[3,4], Nick M. Ashton[5], Joan O. Grimalt[6], Hyuna Kim[7,8], Kyung-Sook Yun[7,9], Philip L. Gibbard[10], Chris B. Stringer[4], Axel Timmermann[7,9*], Polychronis C. Tzedakis[1*]

Science. science.org/doi/10.1126/science.adf4445 (2023)

Affiliations:

[1]Environmental Change Research Centre, Department of Geography, University College London; London WC1E 6BT, UK

[2]Department of Earth Sciences, University of Cambridge; Cambridge CB2 3EQ, UK

[3]Institute of Archaeology, University College London; London WC1H 0PY, UK

[4]Centre for Human Evolution Research, The Natural History Museum; London SW7 5BD, UK

[5]Department of Britain, Europe and Prehistory, British Museum; London N1 5QJ, UK

[6]Department of Environmental Chemistry, Institute of Environmental Assessment and Water Research (IDAEA), Spanish Council for Scientific Research (CSIC); Barcelona 08034, Spain

[7]Institute for Basic Science, Center for Climate Physics; Busan 46241, South Korea

[8]Department of Climate System, Pusan National University, Busan 46241, South Korea.

[9]Pusan National University; Busan 46241, South Korea

[10]Scott Polar Research Institute, University of Cambridge; Cambridge CB2 1ER, UK

*Corresponding authors. Emails: p.c.tzedakis@ucl.ac.uk (P.C.T); axel@ibsclimate.org (A.T.)

Abstract: The oldest known hominin remains in Europe (~1.5 to ~1.1 million years ago [Ma]) have been recovered from Iberia where paleoenvironmental reconstructions have indicated warm and wet interglacials and mild glacials, supporting the view that once established, hominin populations persisted continuously. We report analyses of marine and terrestrial proxies from a deep-sea core on the Portuguese Margin that show the presence of pronounced millennial-scale climate variability during a glacial period ~1.154 to ~1.123 Ma, culminating in a terminal stadial cooling comparable to the most extreme events of the last 400 thousand years. Climate envelope model simulations reveal a drastic decrease in early hominin habitat suitability around the Mediterranean during the terminal stadial. We suggest that the extreme conditions led to the depopulation of Europe, perhaps lasting for several successive glacial-interglacial cycles.

One-Sentence Summary: An intensification of glaciation ~1.15 million years ago challenges the idea of permanent early hominin occupation of Europe

Main Text: The earliest published fossil hominin (*Homo* sp.) evidence in Europe is a mandible and a hand phalanx found with stone tools at the site of Sima del Elefante, Sierra de Atapuerca, northern Spain (*1, 2*), as well as a deciduous molar and stone tools from the sites of Barranco León and Fuente Nueva 3, Guadix-Baza Basin, southeastern Spain (*3, 4*). Analysis of traits of the Sima del Elefante hominin suggests a possible Eurasian (rather than African) evolutionary origin (*5*) for the population it represents. Given that hominins were present at Dmanisi, Georgia ~1.8 Ma (*6*), dispersal into Europe could have taken place at any time after that, but sites in Italy and Spain yielding stone tools and human remains over a broad time-window of ~1.6 to ~1.1 Ma, indicate a delay of ~200 thousand years (kyr). (Fig. 1; table S1; *7*). This dispersal lag may be attributed to a period of cooler interglacials ~1.8 to ~1.6 Ma, which in turn may be related to the 1.2-million-year (Myr) amplitude modulation of the obliquity cycle (*8*).

Considerable disagreement remains on whether early hominin occupation was permanent (*9-11*) or restricted to interglacials, implying that southern Europe was repeatedly colonized from Southwest Asia (*12-14*). Although various factors (geographical, biological, techno-cultural, demographic) influence hominin occupation patterns, environmental conditions ultimately act as a limiting factor. Therefore reconstructions of the climatic background to hominin occupation can constrain the likelihood of different scenarios.

Before 1.2 Ma, glacial-interglacial cycles occurred with a period of ~41 kyr, with maximum ice volumes ranging between one half and one third of the Last Glacial Maximum value (*15, 16*). The less extensive ice sheets and shorter glacial periods of the Early Pleistocene have been linked to smaller decreases in temperature compared with those of the Middle and Late Pleistocene. Nonetheless, North Atlantic records point to the occurrence of iceberg discharges

from marine-terminating ice sheets and disruptions of the Atlantic meridional overturning circulation (AMOC) during the interval ~1.43 to ~1.25 Ma (*17-20*), but their downstream impacts on European climate remain largely unknown. A lengthening and intensification of glacial-interglacial cycles took place over the so-called Early–Middle Pleistocene Transition (~1.25 to ~0.70 Ma [*21*]), after which ice volume varied with a dominant ~80-120-kyr periodicity.

Paleoenvironmental reconstructions based on animal and plant remains from the Atapuerca and Guadix-Baza occupation levels indicate a diverse mosaic of Mediterranean and temperate woodlands, open shrublands and extensive wetlands, with mean annual temperatures similar to those of the present, but higher mean annual precipitation (*10, 22-25*). The presence of thermophilous species within a mosaic of woodland and open habitats throughout the Sima del Elefante sequence has been used to infer relative ecological stability during both interglacials and glacials and to argue for the continuity of occupation (*10*), but stratigraphical hiatuses and preservation biases may have led to intermittent representation, complicating such interpretations. Early Pleistocene pollen sequences are available from northeastern Spain (*26*), but are fragmentary and lack precise chronologies. In the Guadix-Baza Basin, the Palominas pollen record contains a succession of ~10 forest and open vegetation phases, representing interglacial and glacial periods, respectively (*27*). In the absence of independent chronological controls, biostratigraphical correlations point to the record extending from ~1.6 to ~1.2 Ma (*27*). Pollen-based climate reconstructions suggest mean annual precipitation levels during glacials similar to modern, and higher during interglacials; temperature reconstructions for both glacials and interglacials indicate values similar to present (*27*). The implication is that these conditions

would have allowed hominin populations to persist through glacials and expand during interglacials (*11*).

Assessing climate impacts on human populations

To address the pervasive issues with stratigraphical continuity and chronological control in terrestrial sedimentary sequences, we have undertaken an examination of the paleoenvironmental context during the interval of early human occupation at deep-sea Site U1385 on the southwestern Portuguese margin (*28*) (fig. S1), a prime location for joint marine-terrestrial analyses and correlations (*29-32*). Sites on the southwestern Portuguese margin are also well situated to record past changes in North Atlantic surface and deep-ocean circulation: during Marine Isotope Stage (MIS) 3 (59 to24 thousand years ago [ka]), the oxygen isotopic composition of planktic foraminifera ($\delta^{18}O_{planktic}$) closely matched the Greenland temperature record, with abrupt transitions marking the onset and end of interstadials, while the oxygen isotopic composition of benthic foraminifera ($\delta^{18}O_{benthic}$) resembled the Antarctic temperature record, both in its shape and phasing relative to Greenland (*33*). This asynchronous phasing between $\delta^{18}O_{planktic}$ and $\delta^{18}O_{benthic}$ has been interpreted as a fingerprint of AMOC changes associated with interhemispheric heat transport and the bipolar-seesaw (*31*). Here, we focus on reconstructing sea and land changes during two time-windows of the interval of early hominin occupation, representing distinct climatic contexts: a 41-kyr cycle, MIS 43 to 42 (~1.380 to ~1.338 Ma) and one cycle from the Early–Middle Pleistocene Transition, MIS 35 to 34 (~1.192 to ~1.123 Ma). Analyses (*7*) were undertaken with respect to (i) $\delta^{18}O_{planktic}$ and $\delta^{18}O_{benthic}$, reflecting changes in surface-water conditions, and global ice-volume and deep-water hydrography, respectively; (ii) the relative composition of C37 unsaturated alkenones, reflecting

surface-water conditions; (iii) pollen content, providing an integrated picture of regional vegetation changes in southwestern Portugal; and (iv) x-ray fluorescence (XRF) sediment composition changes, reflecting variations in the relative proportion of detrital (Zr) and biogenic (Sr) sediment supply.

To assess and further quantify the climate impact on human occupation, we develop a climate envelope model that is based on climate data from a 2-Myr transient coupled general circulation model simulation (*34*) and a new database of early hominin sites for Europe and Southwest Asia (table S1) (*7*). This model, which calculates hominin habitat suitability as a function of net primary productivity and minimum annual temperature, is then forced with the respective climate data obtained from a freshwater perturbation model experiment (*7*).

Paleoenvironmental reconstructions

Figure 2 (right) shows the results of our analyses for the interval MIS 43 to 42. The onset of warm conditions occurred at ~1.380 Ma marked by a decrease in detrital sediment supply and a shift to higher alkenone-based sea-surface temperature (SST) and temperate tree-pollen values, while sea level was gradually rising. A decrease in summer insolation at ~1.370 Ma led to an expansion of heathland pollen, reflecting moisture availability under reduced summer evaporation regimes in Portugal (*35*), but steppe-pollen values remained low. Peak interglacial conditions occurred at~1.366 to ~1.353 Ma when SSTs reached 20°C and values of deciduous oak and Mediterranean sclerophyll pollen exceeded 40%. Subsequently, benthic and planktic $\delta^{18}O$ values gradually increased, mirrored by a gradual decline in SST and temperate tree-pollen

values. The MIS 42 glacial (~1.350 to ~1.338 Ma) contained a series of small, centennial-scale oscillations in $\delta^{18}O_{planktic}$ and SST and an increase in steppe pollen percentages.

For the second time-window, MIS 35 to 34 (Fig. 2, left), all proxies indicate the onset of MIS 35 at ~1.192 Ma, with interglacial conditions extending over two precessional cycles until ~1.154 Ma. The pollen record shows two temperate tree maxima followed by expansions of heathland, suggesting continued moisture availability, but not an intervening increase in steppe pollen frequencies. The long MIS 35 (~1.192 to ~1.154 Ma) interglacial was succeeded by a long MIS 34 glacial (~1.154 to ~1.123 Ma), together forming an unusually protracted climate cycle (*15, 36*) characterized by weak eccentricity forcing (Fig. 2a, left). MIS 34 is marked by the occurrence of four stadials and interstadials from ~1.154 to ~1.127 Ma, similar to the Middle and Late Pleistocene millennial-scale climate variability, including abrupt interstadial onsets and asynchronous phasing of the planktic and benthic $\delta^{18}O$ curves, bearing the fingerprint of the bipolar-seesaw (*31, 33*). A large increase in the abundance of tetra-unsaturated C37 alkenones ($\%C_{37:4}$), indicating the advection of low-salinity polar water masses to the Portuguese margin (*37, 38*), was accompanied by major decrease in SST, thermocline cooling (*39*), activation of the bipolar seesaw and maximum expansion of steppe communities at ~1.127 Ma, ushering in a terminal stadial of extreme cold and arid conditions that persisted for 4 kyr before the transition into MIS 33.

Long interglacials and contrasting glacials

Reconstructions from large mammal remains across the western Paleoarctic indicate alternating open savannah and forested savannah landscapes from ~1.8 to ~1.2 Ma, with increased habitat

variability from ~1.2 to ~0.9 Ma; the large diversity of resources especially along river systems and coastal plains is considered to have supported hominin dispersal and occupation during both interglacials and glacials (*40*). Our results partly support this view. Both of the interglacial periods we examined (Fig. 2) were characterized by the persistence of mild and relatively stable conditions with a mosaic of Mediterranean plant communities and open habitats, representing long windows of opportunity for hominin dispersal and occupation. The evidence from the two glacials, however, reveals distinct environmental conditions.

The MIS 42 glacial interval was short (~12 kyr) with subdued centennial-scale SST oscillations (16° to 12°C) and steppe vegetation communities with residual woodland (apart from a brief event with lower SST (9°C) and higher steppe values). The absence of $C_{37:4}$ suggests minimal advection of cold and fresh polar water masses. The overall environmental conditions correspond to terrestrial reconstructions from Iberia (*27*), indicating relatively mild glacials before 1.2 Ma that would not present barriers to hominin dispersal and occupation. By contrast, MIS 34 was a long glacial (~31 kyr) with a series of pronounced and increasingly colder stadial-interstadial oscillations as low eccentricity allowed the continued growth of ice sheets under the influence of internal climate feedbacks (*41*). This culminated at ~1.127 Ma in a long terminal stadial sustained by meltwater from disintegrating ice sheets, leading to (i) AMOC weakening as suggested by negative $\delta^{13}C_{\textit{Cibicidioides}}$ anomalies (Fig. 3c); and (ii) cold (SST 5.6°C) and arid (maximum steppe pollen 65%) conditions comparable to the most extreme events of the last 400 kyr (at ~345, ~265 and ~155 ka) recorded on the southwestern Portuguese margin (fig. S2).

The first major glaciation of the Early–Middle Pleistocene Transition is traditionally considered to have occurred during MIS 22, around 0.9 Ma (*21*). However, the Site ODP677 record from

the eastern Eequatorial Pacific shows a shift towards larger $\delta^{18}O_{benthic}$ values in MIS 34 (*15*), implying increasing global ice volume, although this is not as clear in the deconvolved $\delta^{18}O$ of seawater in Site ODP1123 from the southwest Pacific (*16*) (Fig. 3g). In North America, ice from the Keewatin ice center became more extensive during the pre-Illinoian G glaciation, which includes MIS 34 (*42, 43*). Compilation of sediment volumes and ice-rafted detritus records along the northeast Atlantic continental margin indicate large-scale ice sheet activity in the Kara–Barents-Sea–Svalbard region and more restricted Fennoscandian and British-Irish ice sheets from ~2.7 to ~1.5 Ma; while an extensive Kara–Barents-Sea–Svalbard ice sheet persisted over the interval ~1.5 to ~0.8 Ma, glacial activity intensified around the North Sea, with ice sheets coalescing during peak glaciations (*44*). More specifically, there is evidence of Fennoscandian and British-Irish ice sheets expansion ~1.2 to ~1.1 Ma, with the Fedje Till in the Norwegian Channel (*45, 46*), influx of glaciofluvial deposits from Britain in the central North Sea (*47*), and glacial erratics in the Hattem Beds in the northern Netherlands and adjacent Germany during the Menapian cold Stage, which has been broadly correlated with MIS 34 (*43, 47-49*).

Considering the interval from 1.4 to ~0.8 Ma (Fig. 3, b and e), MIS 34 stands out in the U1385 XRF-record (*28*) as an extended period with pronounced Zr/Sr peaks, indicating increases in detrital sediment supply during cold stadials. This compares with results from Site U1308 located near the center of the the so-called 'ice-rafted detritus belt' of the North Atlantic, which shows high MIS 34 XRF Si/Sr values, reflecting increased delivery of detrital silicate minerals (*18*) of the same order as those from MIS 22. Lithological changes in core MD01-2448 in the Bay of Biscay also show a prominent peak in terrigenous fluxes in MIS 34, suggesting ice-rafted material (*50*), whereas the ice-rafted detritus record from Site ODP983 south of Iceland shows a

series of peaks during MIS 34, but whose absolute values do not stand out relative to those of other glacials (*20*).

Previously published North Atlantic SST reconstructions do not show particularly extreme cooling during MIS 34 (fig. S3), but they are of low temporal resolution or do not capture the entire MIS 34 period. Rodrigues *et al*. (*51*) observed that the major cooling events at ~265 and ~155 ka on the southwestern Portuguese margin were amplified relative to those recorded in the central North Atlantic and suggested that the subpolar front may have been deflected southward in the eastern North Atlantic, with the Portugal Current transporting cold water to the vicinity of Site U1385. Climate models simulating the distribution of glacial meltwater in the North Atlantic show the most pronounced negative salinity anomalies on the eastern boundary and along the Iberian Peninsula (*52*), and this is supported by large negative oxygen isotope excursions in deglacial speleothem records from Iberia (*53*), representing meltwater source effects. It is possible that a similar advection of meltwater towards the Portuguese margin occurred during the terminal stadial of MIS 34, as indicated by our $\%C_{37:4}$ record (Fig. 2f, left), which may have contributed to a regional stratification-driven amplification of negative SST anomalies relative to the open North Atlantic. However, prominent MIS 34 changes are also observed beyond the Portuguese margin, suggesting wider-scale impacts, in contrast to the eastern-amplification view: (i) Over the interval 1.4 to ~0.8 Ma, the $\delta^{13}C_{\textit{Cibicidioides}}$ record of Site DSDP607 (*54*) in the central North Atlantic shows the largest reductions in MIS 34 and then MIS 24 and 22, similar to the $\delta^{13}C_{\textit{Cibicidioides}}$ record of U1385 (*28*), pointing to step changes in deep-ocean circulation (Fig. 3, c and d); (ii) South Atlantic Site ODP1090 has the lowest recorded SST (2°C; Fig. 3f) of the last 3.5 Myr in MIS 34 together with a major increase in $\%C_{37:4}$, indicating a large expansion of polar waters into the sub-Antarctic region (*55*); (iii) In

southeastern Europe, a pollen sequence of the last 1.36 Myr from Lake Ohrid (*56*) reveals a step change in the intensity and duration of glacials at MIS 34 (Fig. 3a): Whereas earlier glacials were characterized by short expansions of herbs, MIS 34 had sustained high abundances of herbs reaching 85% of total pollen, indicating longer and colder-drier conditions across southern Europe. Taken together, the evidence from Europe and the Atlantic suggests an intensification of millennial-scale climate variabilty and glaciation during MIS 34, which we attribute to its long duration that allowed the expansion of ice sheets, and a subsequent large terminal meltwater release during the deglaciation.

Implications for early hominin occupation in Europe

The picture that emerges for the interval of hominin presence before 1.15 Ma is one of long and stable interglacial conditions and short glacials that would have allowed hominin establishment and occupation. However, the character of glacial periods changed at MIS 34. Its pervasive climatic instability would have placed hominin populations under considerable stress. The likely much lower carrying capacity of the environment would have challenged small hunter-gatherer bands, compounded by the likelihood that early hominins lacked sufficient fat insulation and the means to make fire, effective clothing or shelters (*57, 58*), leading to much lower population resilience. The terminal stadial event, with an abrupt drop in southwestern Portuguese margin SSTs of ~7°C represents a drastic climate disruption, which likely affected climate and vegetation patterns across southern Europe with potential implications for early hominin occupation.

To further explore and quantify the possible impacts of this event on early hominin habitability, we conducted a realistic climate model simulation with the Community Earth System Model (CESM), version 1.2 under MIS 34 boundary conditions. Ice sheets were prescribed from a modelling study (*59*), which simulated geographically more restricted European ice sheets compared with the glacial evidence discussed above. The numerical experiment (*7*) mimics a terminal stadial event by applying anomalous deglacial freshwater forcing to the northern North Atlantic, corresponding to a 23 m sea-level equivalent, which is at the low end of MIS 34 ice-volume estimates (*16*). In response to the freshwater perturbation, the AMOC weakens by about 95% and SSTs over the west Iberian margin drop by ~3°C – a fraction of the amplitude of the reconstructed temperature anomaly (Fig. 4c). The simulation, therefore, represents a conservative estimate of the climatic changes that occurred during the terminal stadial event. To estimate the corresponding impact on early human occupation of Europe, we developed a climate envelope model (*7*) that links climatic data (minimum annual temperature and net primary productivity) from a transient Pleistocene simulation (*34*) with fossil and archeological evidence of human occupation in Europe and Southwest Asia covering the time period from 2.0 to 0.7 Ma (table S1) (*7*). The climate envelope model is then used to determine how the simulated terminal stadial climate evolution at every grid point impacted the habitat suitability. The results (Fig. 4, b and d) show a massive drop in habitat suitability around the Mediterranean by more than 50% around 1.117 Ma on the model timescale (corresponding to 1.125 Ma on the U1385 timescale), which is absent in the transient Pleistocene simulation without the millennial-freshwater perturbation. Climate conditions move far away from the preferred climate niche of early European hominins (Fig. 4b and fig. S4). Lasting for about 4 kyr, this event triggered large-scale shifts in vegetation and ecosystems, as documented by the 45% increase of steppe pollen at Site

U1385 and the simulated reduction of 50% in net primary production (fig. S5) over the Iberian Peninsula.

The climatic instability of MIS 34 and the severity of its terminal stadial emerging from this study imply that Iberia, and more generally southern Europe, was depopulated at least once in the Early Pleistocene. Dennell *et al*. (*13*, p. 1514) suggested that the question "When was Europe first colonized?" might be rephrased "How often was Europe uninhabited after hominins first entered it?" We propose that the question may be further qualified by adding "and for how long [was Europe uninhabited]?". While the simulated habitat suitability rebounds following the terminal stadial perturbation (Fig. 4d), Fig. 1 and table S1 hint at a possible longer-lasting hiatus in European and Southwest Asian occupation. If Southwest Asia was depopulated during MIS 34, reoccupation of Europe may have been delayed potentially until as late as MIS 25 or, after the marked glaciation of MIS 22, during MIS 21. This hypothesis can be tested through archaeological or hominin sites with robust chronological constraints. If there was the extirpation of hominins in Europe for such an extended period, it implies that repopulation was by *Homo antecessor*, which may have been a more resilient species with evolutionary or behavioral changes that allowed survival under the increasing intensity of glacial conditions.

References and Notes

1. E. Carbonell, J. M. Bermúdez de Castro, J. M. Parés, A. Pérez-González, G. Cuenca-Bescós, A. Ollé, M. Mosquera, R. Huguet, J. van der Made, A. Rosas, R. Sala, J. Vallverdú, N. García, D. E. Granger, M. Martinón-Torres, X. P. Rodríguez, G. M. Stock, J. M. Vergès, E. Allué, F. Burjachs, I. Cáceres, A. Canals, A. Benito, C. Díez, M. Lozano, A.

Mateos, M. Navazo, J. Rodríguez, J. Rosell, J. L. Arsuaga, The first hominin of Europe. *Nature* **452**, 465-470 (2008).

2. C. Lorenzo, A. Pablos, J. M. Carretero, R. Huguet, J. Valverdú, M. Martinón-Torres, J. L. Arsuaga, E. Carbonell, J. M. Bermúdez de Castro, Early Pleistocene human hand phalanx from the Sima del Elefante (TE) cave site in Sierra de Atapuerca (Spain). *J. Hum. Evol*. **78**, 114-121 (2015).

3. O. Oms, J. M. Parés, B. Martínez-Navarro, J. Agustí, I. Toro, G. Martinez-Fernández, A. Turq, Early human occupation of Western Europe: paleomagnetic dates of two paleolithic sites in Spain. *Proc. Natl Acad. Sci. U.S.A.* **97**, 10666-10670 (2000).

4. I. Toro-Moyano, B. Martínez-Navarro, J. Agustí, C. Souday, J. M. Bermúdez de Castro, M. Martinón-Torres, B. Fajardo, M. Duval, C. Falguères, O. Oms, J. M. Parés, P. Anadón, R. Julià, J. M. García-Aguilar, A.-M. Moigne, M. P. Espigares, S. Ros-Montoya, P. Palmqvist, The oldest human fossil in Europe, from Orce (Spain). *J. Hum. Evol.* **65**, 1-9 (2013).

5. J. M. Bermúdez de Castro, M. Martinón-Torres, A. Gómez-Robles, L. Prado-Simón, L. Martín-Francés, M. Lapresa, A. Olejniczak, E. Carbonell, The Early Pleistocene human mandible from Sima del Elefante (TE) cave site in Sierra de Atapuerca (Spain): a comparative study. *J. Hum. Evol.* **61**, 1-11 (2011).

6. D. Lordkipanidze, T. Jashashvili, A. Vekua, M. S. Ponce de León, C. P. E. Zollikofer, G. P. Rightmire, H. Pontzer, R. Ferring, O. Oms, M. Tappen, M. Bukhsianidze, J. Agusti, R. Kahlke, G. Kiladze, B. Martinez-Navarro, A. Mouskhelishvili, M. Nioradze, L. Rook, Post-cranial evidence from early *Homo* from Dmanisi, Georgia. *Nature* **449**, 305-310 (2007).

7. Materials and Methods are available as supplementary materials.

8. T. Mitsui, P. C. Tzedakis, E. W. Wolff, Insolation evolution and ice volume legacies determine interglacial and glacial intensity. *Clim. Past* **18**, 1983-1996 (2022).

9. J. Garcia, K. Martínez, E. Carbonell, Continuity of the first human occupation in the Iberian Peninsula: Closing the archaeological gap. *C. R. Palevol*. **10**, 279-284 (2011).

10. J. Rodríguez, F. Burjachs, G. Cuenca-Bescós, N. García, J. Van der Made, A. Pérez González, H.-A. Blain, I. Expósito, J. M. López-García, M. García Antón, E. Allué, I. Cáceres, R. Huguet, M. Mosquera, A. Ollé, J. Rosell, J. M. Parés, X. P. Rodríguez, C., Díez, J. Rofes, R. Sala, P. Saladié, J. Vallverdú, M. L. Bennasar, R. Blasco, J. M. Bermúdez de Castro, E. Carbonell, One million years of cultural evolution in a stable environment at Atapuerca (Burgos, Spain). *Quatern. Sci. Rev*. **30**, 1396-1412 (2011).

11. Y. Altolaguirre, J. M. Postigo-Mijarra, E. Barrón, J. S. Carrión, S. A. G. Leroy, A. A. Bruch, An environmental scenario for the earliest hominins in the Iberian Peninsula: early Pleistocene palaeovegetation and palaeoclimate. *Rev. Palaeobot. Palynol*. **260**, 51-64 (2019).

12. R. W. Dennell, Dispersal and colonization, long and short chronologies: how continuous is the Early Pleistocene record for hominids outside East Africa? *J. Hum. Evol.* **45**, 421-440 (2003).

13. R. W. Dennell, M. Martinón-Torres, J. M. Bermúdez de Castro, Hominin variability, climatic instability and population demography in Middle Pleistocene Europe. *Quatern. Sci. Rev*. **30** 1511-1524 (2011).

14. K. MacDonald, M. Martinón-Torres, R. W. Dennell, J. M. Bermúdez de Castro, Discontinuity in the record for hominin occupation in south-western Europe: implications for occupation of the middle latitudes of Europe. *Quatern. Int*. **271**, 84-97 (2012).

15. N. J. Shackleton, A. Berger, W. R. Peltier, An alternative astronomical calibration of the lower Pleistocene timescale based on ODP Site 677. *Trans. R. Soc. Edin., Earth Sci.* **81**, 251-261 (1990).

16. H. Elderfield, P. Ferretti, M. Greaves, S. Crowhurst, I. N. McCave, D. Hodell, A. M. Piotrowski, Evolution of ocean temperature and ice-volume through the Mid-Pleistocene climate transition. *Science* **337**, 704-709 (2012).

17. M. E. Raymo, K. Ganley, S. Carter, D. W. Oppo, J. McManus, Millennial-scale climate instability during the early Pleistocene epoch. *Nature* **392**, 699-702 (1998).

18. D. A. Hodell, J. E. T. Channell, J. H. Curtis, O. E Romero, U. Rohl, Onset of "Hudson Strait" Heinrich events in the eastern North Atlantic at the end of the middle Pleistocene transition (640 ka)? *Paleoceanography* **23,** PA4218 (2008).

19. B. Birner, D. A. Hodell, P. C. Tzedakis, L. C. Skinner, Similar millennial climate variability on the Iberian margin during two early Pleistocene glacials and MIS 3. *Paleoceanography* **31**, 203-217 (2016).

20. S. Barker, A. Starr, J. van der Lubbe, A. Doughty, G. Knorr, S. Conn, S. Lordsmith, L. Owen, A. Nederbragt, S. Hemming, I. Hall, L. Levay, M. A. Berke, L. Brentegani, T. Caley, A. Cartagena-Sierra, C. D. Charles, J. J. Coenen, J. G. Crespin, A. M. Franzese, J. Gruetzner, X. Han, S. K. V. Hines, F. J. Jimenez Espejo, J. Just, A. Koutsodendris, K. Kubota, N. Lathika, R. D. Norris, T. Periera Dos Santos, R. Robinson, J. M. Rolison, M. H. Simon, D. Tangunan, M. Yamane, H. Zhang; IODP Exp 361 Shipboard Scientific Party, Persistent influence of precession on northern ice sheet variability since the early Pleistocene. *Science* **376**, 961-967 (2022).

21. P. U. Clark, D. Archer, D. Pollard, J. D. Blum, J. A. Rial, V. Brovkin, A. C. Mix, N. G. Pisias, M. Roy, The middle Pleistocene transition: characteristics, mechanisms, and

implications for long-term changes in atmospheric pCO_2. *Quatern. Sci. Rev*. **25**, 3150-3184 (2006).

22. H.-A. Blain, S. Bailon, G. Cuenca-Bescós, M. Bennàsar, J. Rofes, J. M. López-García, R. Huguet, J. L. Arsuaga, J. M. Bermúdez de Castro, E. Carbonell, Climate and environment of the earliest West European hominins inferred from amphibian and squamate reptile assemblages: Sima del Elefante Lower Red Unit, Atapuerca, Spain. *Quatern. Sci. Rev*. **29**, 3034-3044 (2010).

23. C. Sánchez-Bandera, O. Oms, H.-A. Blain, I. Lozano-Fernández, J. F. Bisbal-Chinesta, J. Agustí, J. Saarinen, M. Fortelius, S. Titton, A. Serrano-Ramos, C. Luzón, J. Solano-García, D. Barsky, J. M. Jiménez-Arenas, New stratigraphically constrained palaeoenvironmental reconstructions for the first human settlement in Western Europe: The Early Pleistocene herpetofaunal assemblages from Barranco Léon and Fuente Nueva 3 (Granada, SE Spain) *Quatern. Sci. Rev*. **243**, 106466 (2020).

24. J. Saarinen, O. Oksanen, I. Žliobaitė, M. Fortelius, D. DeMiguel, B. Azanza, H. Bocherens, C. Luzón, J. Solano-García, J. Yravedra, L. A. Courtenay, H.-A. Blain, C. Sánchez-Bandera, A. Serrano-Ramos, J. J. Rodriguez-Alba, S. Viranta, D. Barsky, M. Tallavaara, O. Oms, J. Agustí, J. Ochando, J. S. Carrión, J. M. Jiménez-Arenas, Pliocene to Middle Pleistocene climate history in the Guadix-Baza Basin, and the environmental conditions of early *Homo* dispersal in Europe. *Quatern. Sci. Rev*. **268** 107132 (2021).

25. J. Ochando, J. Carrión, Y. Altolaguirre, M. Munuera, G. Amorós, G. Jiménez-Moreno, J. Solano-García, D. Barsky, C. Luzón, C. Sánchez-Bandera, A. Serrano-Ramos, I. Toro-Moyano, J. Saarinen, H.-A. Blain, H. Bocherens, O. Oms, J. Agustí, M. Fortelius, J. M. Jiménez-Arenas, Palynological investigations in the Orce Archaeological Zone., Early Pleistocene of southern Spain. *Rev. Palaeobot. Palynol*. **304**, 104725 (2022).

26. P. González-Sampériz, S. A. G. Leroy, J. S. Carrión, S. Fernández, M. García-Antón, M. J. Gil-García, P. Uzquiano, B. Valero-Garcés, I. Figueiral, Steppes, savannahs, forests and phytodiversity reservoirs during the Pleistocene in the Iberian Peninsula. *Rev. Palaeobot. Palynol*. **162**, 427-457 (2010).

27. Y. Altolaguirre, A. A. Bruch, L. Gibert, A long early Pleistocene pollen record from Baza Basin (SE Spain): major contributions to the palaeoclimate and palaeovegetation of southern Europe. *Quatern. Sci. Rev*. **231**, 106-199 (2020).

28. D. A. Hodell, S. J. Crowhurst, L. Lourens, V. Margari, J. Nicolson, J. E. Rolfe, L. C. Skinner, N. C. Thomas, P. C. Tzedakis, M. J. Mleneck-Vautravers, E. W. Wolff, A 1.5-Million-Year Record of Orbital and Millennial Climate Variability in the North Atlantic. *Clim. Past* **19**, 607-636 (2023).

29. N. J. Shackleton, M. Chapman, M. F. Sánchez-Goñi, D. Pailler, Y. Lancelot, The classic Marine Isotope Substage 5e. *Quatern. Res*. **58**, 14-16 (2002).

30. P. C. Tzedakis, K. H. Roucoux, L. de Abreu, N. J. Shackleton, The duration of forest stages in southern Europe and interglacial climate variability. *Science* **306**, 2231-2235 (2004).

31. V. Margari, L. C. Skinner, P. C. Tzedakis, A. Ganopolski, M. Vautravers, N. J. Shackleton, The nature of millennial-scale climate variability during the past two glacial periods. *Nat. Geosci.* **3,** 127-133 (2010).

32. M. F. Sánchez Goñi, S. Desprat, W. J. Fletcher, C. Morales-Molino, F. Naughton, D. Oliveira, D. H. Urrego, C. Zorzi, Pollen from the Deep-Sea: A Breakthrough in the Mystery of the Ice Ages. *Front. Plant Sci*. **9-38** doi: 10.3389/fpls.2018.00038 (2018).

33. N. J. Shackleton, M. A. Hall, E. Vincent, Phase relationships between millennial-scale events 64,000-24,000 years ago. *Paleoceanography* **15**, 565-569 (2000).

34. A. Timmermann, K.-S. Yun, P. Raia, J. Ruan, A. Mondanaro, E. Zeller, C. Zollikofer, M. Ponce de León, D. Lemmon, M. Willeit, A. Ganopolski, Climate effects on archaic human habitats and species successions. *Nature* **604**, 495-501 (2022).

35. V. Margari, L. C. Skinner, D. A. Hodell, B. Martrat, S. Toucanne, J. O. Grimalt, P. L. Gibbard, J. P. Lunkka, P. C. Tzedakis, Land-ocean changes on orbital and millennial timescales and the penultimate glaciation. *Geology* **42**,183-186 (2014).

36. E. L. McClymont, S. M. Sosdian, A. Rosell-Melé, Y. Rosenthal, Pleistocene sea-surface temperature evolution: Early cooling, delayed glacial intensification, and implications for the mid-Pleistocene climate transition. *Earth-Sci. Rev*. **123**, 173-193 (2013).

37. E. Bard, F. Rostek, J.-L. Turon, S. Gendreau, Subtropical Northeast Atlantic Hydrological Impact of Heinrich Events in the Subtropical Northeast Atlantic. *Science* **289**, 1321-1324 (2000).

38. B. Martrat, J. O. Grimalt, N. J. Shackleton, L. de Abreu, M. A. Hutterli, T. F. Stocker, Four climate cycles of recurring deep and surface water destabilizations on the Iberian margin. *Science* **317,** 502-507 (2007).

39. A. Bahr, S. Kaboth, D. Hodell, C. Zeeden, J. Fiebig, O. Friedrich, Oceanic heat pulses fueling moisture transport towards continental Europe across the mid-Pleistocene transition. *Quatern. Sci. Rev*. **179**, 48-58 (2018).

40. R.-D. Kahlke, N. García, D. S. Kostopoulos, F. Lacombat, A. M. Lister, P. P. A. Mazza, N. Spassov, V. V. Titov, Western Palaearctic palaeoenvironmental conditions during the Early and early Middle Pleistocene inferred from large mammal communities, and implications for hominin dispersal in Europe. *Quatern. Sci. Rev*. **30**, 1368-1395 (2011).

41. L. E. Lisiecki, Links between eccentricity forcing and the 100,000-year glacial cycle. *Nat. Geosci.* **3,** 349-352 (2010).

42. R. W. Barendregt, A. Duk-Rodkin, “Chronology and extent of Late Cenozoic ice sheets in North America: A magnetostratigraphical assessment” in *Developments in Quaternary Sciences,* vol. 15, *Quaternary Glaciations – Extent and Chronology - A Closer Look*, J. Ehlers, P. L. Gibbard, P. D. Hughes, Eds. (Elsevier, 2011), pp. 419-426.

43. J. Ehlers, P. L. Gibbard, The extent and chronology of Cenozoic Global Glaciation. *Quatern. Int*. **164-165**, 6-20 (2007).

44. Ø. F. Lien, B. O. Hjelstuen, X. Zhang, H. P. Sejrup, Late Plio-Pleistocene evolution of the Eurasian Ice Sheets inferred from sediment input along the northeastern Atlantic continental margin. *Quatern. Sci. Rev*. **282**, 107433 (2022).

45. H. P. Sejrup, I. Aarseth, H. Haflidason, R. Løvlie, Å. Bra Tien, G. Tjøstheim, C. Forsberg, K. Ellingsen, Quaternary of the Norwegian Channel: glaciation history and palaeoceanography. *Norsk Geol. Tidsskr*. **75**, 65-87 (1995).

46. D. Ottesen, C. L. Batchelor, J. A. Dowdeswell, H. Løseth, Morphology and pattern of Quaternary sedimentation in the North Sea Basin (52–62°N). *Mar. Petrol. Geol*. **98**, 836-859 (2018).

47. J. R. Lee, F. S. Busschers, H. P. Sejrup, Pre-Weichselian Quaternary glaciations of the British Isles, The Netherlands, Norway and adjacent marine areas south of 68°N: implications for long-term ice sheet development in northern Europe. *Quatern. Sci. Rev*. **44**, 213-228 (2012).

48. W. H. Zagwijn, An outline of the Quaternary stratigraphy of The Netherlands. *Geol. Mijnbouw* **64**, 17-24 (1985).

49. C. Laban, J. J. M. van der Meer, “Pleistocene glaciation in the Netherlands” in *Developments in Quaternary Sciences,* vol. 15, *Quaternary Glaciations – Extent and*

Chronology - A Closer Look, J. Ehlers, P. L. Gibbard, P. D. Hughes, Eds. (Elsevier, 2011), pp. 247-260.

50. S. Toucanne, S. Zaragosi, J. F. Bourillet, M. Cremer, F. Eynaud, B. Van Vliet-Lanoë, A. Penaud, C. Fontanier, J. L. Turon, E. Cortijo, Timing of 'Fleuve Manche' discharges over the last 350 kyr: Insights into the European ice-sheet oscillations and the European drainage network from MIS 10 to 2. *Quatern. Sci. Rev*. **28**, 1238-1256 (2009).

51. T. Rodrigues, M. Alonso-García, D. A. Hodell, M. Rufino, F. Naughton, J. O. Grimalt, A. H. L. Voelker, F. Abrantes, A 1-Ma record of sea surface temperature and extreme cooling events in the North Atlantic: A perspective from the Iberian margin. *Quatern. Sci. Rev*. **172**, 118-130 (2017).

52. R. Ivanovic, L. J. Gregoire, A. Burke, A. D. Wickert, P. J. Valdes, H. C. Ng, L. F. Robinson, J. F. McManus, J. X. Mitrovica, L. Lee, J. E. Dentith, Acceleration of northern ice sheet melt induces AMOC slowdown and northern cooling in simulations of the early last deglaciation. *Paleoceanogr*. *Paleoclimatol*. **33**, 807-824 (2018).

53. H. M. Stoll, I. Cacho, E. Gasson, J. Sliwinski, O. Kost, A. Moreno, M. Iglesias, J. Torner, C. Perez-Mejias, N. Haghipour, H. Cheng, R. L. Edwards, Rapid northern hemisphere ice sheet melting during the penultimate deglaciation. *Nat. Commun*. **13**, 3819 (2022).

54. W. F. Ruddiman, M. E. Raymo, D. G. Martinson, B. M. Clement, J. Backman, Pleistocene evolution: ice sheets and North Atlantic Ocean. *Paleoceanography* **4**, 353-412 (1989).

55. A. Martínez-Garcia, A. Rosell-Melé, E. L. McClymont, R. Gersonde, G. H. Haug, Subpolar Link to the Emergence of the Modern Equatorial Pacific Cold Tongue. *Science* **328**, 1550-1553 (2010).

56. T. Donders, K. Panagiotopoulos, A. Koutsodendris, A. Bertini, A. M. Mercuri, A. Masi, N. Combourieu-Nebout, S. Joannin, K. Kouli, I. Kousis, O. Peyron, P. Torri, A. Florenzano,

A. Francke, B. Wagner, L. Sadori, 1.36 million years of Mediterranean forest refugium dynamics in response to glacial–interglacial cycle strength. *Proc. Natl Acad. Sci. U.S.A.* **118**, e2026111118 (2021).

57. W. Roebroeks, P. Villa, On the earliest evidence for habitual use of fire in Europe. *Proc. Natl Acad. Sci. U.S.A.* **108**, 5209-5214 (2011).

58. R. T. Hosfield, Walking in a winter wonderland? Strategies for Early and Middle Pleistocene survival in midlatitude Europe. *Curr. Anthropol*. **57**, 653-682 (2016).

59. M. Willeit, A. Ganopolski, R. Calov, V. Brovkin, Mid-Pleistocene transition in glacial cycles explained by declining CO_2 and regolith removal. *Sci. Adv*. **5**, eaav7337 (2019).

60. J. Laskar, P. Robutel, F. Joutel, M. Gastineau, A. C. M. Correia, B. Levrard, A long-term numerical solution for the insolation quantities of the Earth. *Astron. Astrophys*. **428**, 261285 (2004).

61. V. Margari, D. A. Hodell, J. O. Grimalt, P. C. Tzedakis, Benthic and planktic oxygen and carbon isotopes, alkenone, pollen, and XRF data at IODP 339-U1385 for MIS 34-35 and MIS 42-43 southern Portuguese Margin. PANGAEA (2023); https://doi.org/10.1594/PANGAEA.961070

62. V. Margari, D. A. Hodell, S. A. Parfitt, N. M. Ashton, J. O. Grimalt, H. Kim, K.-S. Yun, P. L. Gibbard, C. B. Stringer, A. Timmermann, P. C. Tzedakis et al., MIS34 transient climate model simulation data, Institute for Basic Science ICCP data server (2023); https://doi.org/10.22741/iccp.20230006.

63. V. Margari, D. A. Hodell, S. A. Parfitt, N. M. Ashton, J. O. Grimalt, H. Kim, K.-S. Yun, P. L. Gibbard, C. B. Stringer, A. Timmermann, P. C. Tzedakiset al., Matlab code for MIS34 human habitat simulation, Institute for Basic Science. ICCP data server (2023); https://doi.org/10.22741/iccp.20230007.

64. D. Hodell, L. Lourens, S. Crowhurst, T. Konijnendijk, R. Tjallingii, F. Jiménez-Espejo, L. Skinner, P. C. Tzedakis, F. Abrantes, G. D. Acton, C. A. Alvarez Zarikian, A. Bahr, B. Balestra, E. L. Barranco, G. Carrara, E. Ducassou, R. D. Flood, J.-A. Flores, S. Furota, J. Grimalt, P. Grunert, J. Hernández-Molina, J. K. Kim, L. A. Krissek, J. Kuroda, B. Li, J. Lofi, V. Margari, B. Martrat, M. D. Miller, F. Nanayama, N. Nishida, C. Richter, T. Rodrigues, F. J. Rodríguez-Tovar, A. C. F. Roque, M. F. Sanchez Goñi, F. J. Sierro Sánchez, A. D. Singh, C. R. Sloss, D. A. V. Stow, Y. Takashimizu, A. Tzanova, A. Voelker, C. Xuan, T. Williams, A reference time scale for Site U1385 (Shackleton Site) on the SW Iberian margin. *Global Planet. Change* **133**, 49-64 (2015).

65. M. Vautravers, N. J. Shackleton, Centennial scale surface hydrology off Portugal during Marine Isotope Stage 3: Insights from planktonic foraminiferal fauna variability. *Paleoceanography* **21**, PA3004 (2006).

66. D. Hodell, S. Crowhurst, L. Skinner, P. C. Tzedakis, V. Margari, J. E. T. Channell, G. Kamenov, S. Maclachlan, G. Rothwell, Response of Iberian margin sediments to orbital and suborbital forcing over the past 420 ka. *Paleoceanography* **28**, 185-199 (2013).

67. P. C. Tzedakis, R. N. Drysdale, V. Margari, L. C. Skinner, L. Menviel, R. H. Rhodes, A. S. Taschetto, D. A. Hodell, S. J. Crowhurst, J. C. Hellstrom, A. E. Fallick, J. O. Grimalt, J. F. McManus, B. Martrat, Z. Mokeddem, F. Parrenin, E. Regattieri, K. Roe, G. Zanchetta, Enhanced climate instability in the North Atlantic and southern Europe during the Last Interglacial. *Nat. Commun.* **9**, 4235 (2018).

68. A. Cutmore, B. Ausín, M. Maslin, T. Eglinton, D. Hodell, F. Muschitiello, L. Menviel, N. Haghipour, B. Martrat, V. Margari, P. C. Tzedakis, Abrupt intrinsic and extrinsic responses of southwestern Iberian vegetation to millennial-scale variability over the past 28 ka. *J. Quatern. Sci.* **37**, 420-440. https://dx.doi.org/10.1002/jqs.3392 (2021).

69. V. Margari, L. C. Skinner, L. Menviel, E. Capron, R. H. Rhodes, M. J. Mleneck-Vautravers, M. M. Ezat, B. Martrat, J. O. Grimalt, D. A. Hodell, P. C. Tzedakis, Fast and slow components of interstadial warming in the North Atlantic during the last glacial. *Commun. Earth Environment* **1**, 6 (2020).

70. O. Rama-Corredor, A. Cortina, B. Martrat, J. F. Lopez, J. O. Grimalt, Removal of bias in C37 alkenone-based sea surface temperature measurements by high-performance liquid chromatography fractionation. *J. Chromatogr.* A **1567**, 90-98 (2018).

71. S. C. Brassell, G. Eglinton, I. T. Marlowe, U. Pflaumann, M. Sarnthein, Molecular stratigraphy: a new tool for climatic assessment. *Nature* **320**, 129-133 (1986).

72. P. J. Müller, G. Kirst, G. Ruhland, I. Von Storch, A. Rosell-Melé, Calibration of the alkenone paleotemperature index $U^{k'}_{37}$ based on core-tops from the eastern South Atlantic and the global ocean (60°N-60°S). *Geochim. Cosmochim. Ac.* **62**, 1757-1772 (1998).

73. J. Villanueva, C. Pelejero, J. O. Grimalt, Clean-up procedures for the unbiased estimation of C37 alkenone sea surface temperatures and terrigenous n-alkane inputs in paleoceanography. *J. Chromatogr*. *A* **757**, 145-151 (1997).

74. K. J. Wang, Y. Huang, M. Majaneva, S. T. Belt, S. Liao, J. Novak, T. R. Kartzinel, T. D. Herbert, N. Richter, P. Cabedo-Sanz, Group 2i Isochrysidales produce characteristic alkenones reflecting sea ice distribution. *Nat. Commun.* **12**, 15 (2021).

75. L. E. Heusser, W. L. Balsam, Pollen distribution in the N.E. Pacific Ocean. *Quatern. Res*. **7**, 45-62 (1977).

76. G. L. Chmura, A. Smirnov, I. D. Campbell, Pollen transport through distributaries and depositional patterns in coastal waters. *Palaeogeogr. Palaeoclimat. Palaeoecol*. **149,** 257-270 (1999).

77. F. Naughton, M. F. Sanchez Goñi, S. Desprat, J.-L. Turon, J. Duprat, B. Malaizé, C. Joli, E. Cortijo, T. Drago, M. C. Freitas, Present-day and past (last 25 000 years) marine pollen signal off western Iberia. *Mar. Micropaleontol*. **62,** 91-114 (2007).

78. C. Morales-Molino, L., Devaux, M., Georget, V. Hanquiez, M. F. Sánchez-Goñi, Modern pollen representation of the vegetation of the Tagus Basin central Iberian Peninsula). *Rev. Palaeobot. Palynol*. **276,** 104193 (2020).

79. L. E. Lisiecki, M. E.Raymo, A Pliocene-Pleistocene stack of 57 globally distributed benthic $\delta^{18}O$ records. *Paleoceanography* **20**, PA1003 (2005). doi:10.1029/2004PA001071

80. S. Ahn, D. Khider, L. E. Lisiecki, C. E. Lawrence, A probabilistic Pliocene-Pleistocene stack of benthic $\delta^{18}O$ using a profile hidden Markov model. *Dynam. Stat. Clim. Syst*. **2**, 1-16 (2017).

81. T. Konijnendijk, M. Ziegler, L. Lourens, Chronological constraints on Pleistocene sapropel depositions from high-resolution geochemical records of ODP sites 967 and 968. *Newsletters Stratigr*. **47**, 263-282 (2014).

82. T. Konijnendijk, M. Ziegler, L. Lourens, On the timing and forcing mechanisms of late Pleistocene glacial terminations: Insights from a new high-resolution benthic stable oxygen isotope record of the eastern Mediterranean. *Quatern. Sci. Rev.* **129**, 308-320 (2015).

83. W. Roebroeks, T. van Kolfschoten, The earliest occupation of Europe: a short chronology. *Antiquity* **68**, 489-503 (1994).

84. W. Roebroeks, T. van Kolfschoten, Eds., *The Earliest Occupation of Europe: Proceedings of the European Science Foundation Workshop at Tautavel (France) 1993* (Leiden University Press, 1995).

85. C. White, La Grotte du Vallonet: evidence of early hominid activity or natural processes? *Lithics* **16**, 70-77 (1995).

86. J. Madurell-Malapeira, D. M. Alba, R. Minwer-Barakat, J. Aurell-Garrido, S. Moyà-Solà, Early human dispersals into the Iberian peninsula: a comment on Martinez *et al*. (2010) and Garcia *et al*. (2011). *J. Hum. Evol*. **62**, 169-173 (2012).

87. W. Roebroeks, S. Gaudzinski-Windheuser, M. Baales, R-D. Kahle, Uneven data quality and the earliest occupation of Europe—the case of Untermassfeld (Germany). *J. Paleolith. Archaeol.* **1**, 5-31 (2018).

88. P. M. Lubinski, K. Terry, P. T. McCutcheon, Comparative methods for distinguishing flakes from geofacts: a case study from the Wenas Creek Mammoth site. *J. Archaeol. Sci*. **52**, 308-320 (2014).

89. A. Timmermann, T. Friedrich, Late Pleistocene climate drivers of early human migration. *Nature* **538**, 92-95 (2016).

90. A. Berger, Long-term variations of caloric insolation resulting from the earth's orbital elements. *Quatern. Res*. **9**, 139-167 (1978).

91. S. Del Grosso, W. Parton, T. Stohlgren, D. Zheng, D. Bachelet, S. Prince, K. Hibbard, R. Olson, Global potential net primary production predicted from vegetation class, precipitation, and temperature. *Ecology* **89**, 2117-2126 (2008).

92. V. Brovkin, A. Ganopolski, Y. Svirezhev, continuous climate-vegetation classification for use in climate-biosphere studies. *Ecol. Model.* **101**, 251-261 (1997).

93. W. E. Banks, F. d'Errico, A. T. Peterson, M. Vanhaeren, M. Kageyama, P. Sepulchre, G. Ramstein, A. Jost, D. Lunt, Human ecological niches and ranges during the LGM in Europe derived from an application of eco-cultural niche modeling. *J. Archaeol. Sci.* **35**, 481-491 (2008).

94. C. Calenge, G., Darmon, M., Basille, A. Loison, J. M. Jullien, The factorial decomposition of the Mahalanobis distances in habitat selection studies. *Ecology* **89**, 555-566 (2008).

95. T. R. Etherington, Mahalanobis distances and ecological niche modelling: correcting a chi-squared probability error. *Peerj* **7**, e6678 (2019).

96. O. Farber, R. Kadmon, Assessment of alternative approaches for bioclimatic modeling with special emphasis on the Mahalanobis distance. *Ecol. Model.* **160**, 115-130 (2003).

97. A. Tsoar, O., Allouche, O., Steinitz, D. Rotem, R. A Kadmon, comparative evaluation of presence-only methods for modelling species distribution. *Divers. Distrib.* **13**, 397-405 (2007).

98. M. Will, M., Krapp, J. T. Stock, A. Manica, Different environmental variables predict body and brain size evolution in Homo. *Nat. Commun*. **12**, 4116 (2021).

99. E. L. McClymont, A. Rosell-Melé, G. H. Haug, J. M. Lloyd, Expansion of subarctic water masses in the North Atlantic and Pacific oceans and implications for mid-Pleistocene ice sheet growth. *Paleoceanography* **23**, PA4214 (2008).

100. K. T. Lawrence, T. D. Herbert, C. M. Brown, M. E. Raymo, A. M. Haywood, High-amplitude variations in North Atlantic sea surface temperature during the early Pliocene warm period. *Paleoceanography* **24**, PA2218 (2009).

101. K. T. Lawrence, S. Sosdian, H. E. White, Y. Rosenthal, North Atlantic climate evolution through the Plio-Pleistocene climate transitions. *Earth Planet. Sci. Lett*. **300**, 329-342 (2010).

102. B. D. A. Naafs, J. Hefter, R. Stein, Millennial-scale ice rafting events and Hudson Strait Heinrich(-like) Events during the late Pliocene and Pleistocene: a review. *Quatern. Sci. Rev*. **80**, 1-28 (2013).

103. A. H. L. Voelker, E. Salgueiro, T. Rodrigues, F. J. Jimenez-Espejo, A. Bahr, A. Alberto, I. Loureiro, M. Padilha, A. Rebotim, U. Röhl, Mediterranean Outflow and surface water

variability off southern Portugal during the early Pleistocene: A snapshot at Marine Isotope Stages 29 to 34 (1020–1135 ka). *Global Planet. Change* **133**, 223-237 (2015).

104. S. A. Parfitt, N. M. Ashton, S. G. Lewis, R. L. Abel, G. R. Coope, M. H. Field, R. Gale, P. G. Hoare, N. R. Larkin, M. D. Lewis, V. Karloukovski, B. A. Maher, S. M. Peglar, R. C. Preece, J. E. Whittaker, C. B. Stringer, Early Pleistocene human occupation at the edge of the boreal zone in northwest Europe. *Nature* **466**, 229-233 (2010).

105. N. Ashton, S. G. Lewis, I. De Groote, S. M. Duffy, M. Bates, R. Bates, P. Hoare, M. Lewis, S. A. Parfitt, S. Peglar, C. Williams, C. Stringer, Hominin footprints from Early Pleistocene deposits at Happisburgh, UK. *PLOS One* **9 (2)**: e88329 (2014).

106. E. Carbonell, J. M. Bermúdez de Castro, J. L. Arsuaga, E. Allue, M. Bastir, A. Benito, I. Cáceres, T. Canals, J. C. Díez, J. van der Made, M. Mosquera, A. Ollé, A. Pérez-González, J. Rodríguez, X. P. Rodríguez, A. Rosas, J. Rosell, R. Sala, J. Vallverdú, J. M. Vergés, An Early Pleistocene hominin mandible from Atapuerca-TD6, Spain. *Proc. Natl Acad. Sci. U.S.A.* **102**, 5674-5678 (2005).

107. A. Ollé, M. Mosquera, X. P. Rodríguez, A. de Lombera-Hermida, M. D. García-Antón, P. García-Medrano, L. Peña, L. Menéndez, M. Navazo, M. Terradillos, A. Bargalló, B. Márquez, R. Sala, E. Carbonell, The Early and Middle Pleistocene technological record from Sierra de Atapuerca (Burgos, Spain). *Quatern. Int*. **295**, 138-167 (2013).

108. H.-A. Blain, J. A. Cruz Silva, J. M. Jiménez Arenas, V. Margari, K. Roucoux, Towards a Middle Pleistocene terrestrial climate reconstruction based on herpetofaunal assemblages from the Iberian Peninsula: State of the art and perspectives. *Quatern. Sci. Rev*. **191**, 167-188 (2018).

109. M. Duval, L. J. Arnold, M. Demuro, J. M. Parés, I. Campaña, E. Carbonell, J. M. Bermúdez de Castro, New chronological constraints for the lowermost stratigraphic unit of Atapuerca Gran Dolina (Burgos, N Spain). *Quatern. Geochronol*. **71**, 101292 (2022).

110. A. de Lombera-Hermida, A. Bargalló, M. Terradillos-Bernal, R. Huguet, J. Vallverdú, M. D. García-Antón, M. Mosquera, A. Ollé, R. Sala, E. Carbonell, X. P. Rodríguez-Álvarez, The lithic industry of Sima del Elefante (Atapuerca, Burgos, Spain) in the context of Early and Middle Pleistocene technology in Europe. *J. Hum. Evol.* **82**, 95-106 (2015).

111. R. Huguet, J. Vallverdú, X. P. Rodríguez-Álvarez, M. Terradillos-Bernal, A. Bargalló, A. Lombera-Hermida, L. Menéndez, M. Modesto-Mata, J. Van der Made, M. Soto, H.-A. Blain, N. García, G. Cuenca-Bescós, G. Gómez-Merino, R. Pérez-Martínez, I. Expósito, E. Allué, J. Rofes, F. Burjachs, A. Canals, M. Bennàsar, C. Nuñez-Lahuerta, J. M. Bermúdez de Castro, E. Carbonell, Level TE9c of Sima del Elefante (Sierra de Atapuerca, Spain): A comprehensive approach. *Quatern. Int*. **433**, 278-295 (2017).

112. I. Toro-Moyano, D. Barsky, D. Cauche, V. Celiberti, S. Grégoire, F. Lebegue, M. H. Moncel, H. de Lumley, The archaic stone tool industry from Barranco León and Fuente Nueva 3, (Orce, Spain): Evidence of the earliest hominin presence in southern Europe. *Quatern. Int.* **243**, 80-91 (2011).

113. M. Duval, C. Falguères, J.-J. Bahain, R. Grün, Q. Shao, M. Aubert, J.-M. Dolo, J. Agustí, B. Martínez-Navarro, P. Palmqvist, I. Toro-Moyano, On the limits of using combined U-series/ESR method to date fossil teeth from two Early Pleistocene archaeological sites of the Orce area (Guadix-Baza basin, Spain). *Quatern. Res*. **77**, 482-491 (2012).

114. J. Agustí, H.-A. Blain, M. Furió, R. De Marfá, A. Santos-Cubedo, The early Pleistocene small vertebrate succession from the Orce region (Guadix-Baza Basin, SE Spain) and its bearing on the first human occupation of Europe. *Quatern. Int*. **223-224**, 162-169 (2010).

115. H.-A. Blain, I. Lozano-Fernández, J. Agustí, S. Bailon, L. Menéndez Granda, M. P. Espígares Ortiz, S. Ros-Montoya, J. M. Jiménez Arenas, I. Toro-Moyano, B. Martínez-Navarro, R. Sala, Refining upon the climatic background of the Early Pleistocene hominid settlement in western Europe: Barranco Léon and Fuente Nueva-3 (Guadix-Baza Basin, SE Spain). *Quatern. Sci. Rev*. **144**, 132-144 (2016).

116. B. Martínez Navarro, A. Turq, J. A. Ballester, O. Oms, Fuente Nueva-3 (Orce, Granada, Spain) and the first human occupation of Europe. *J. Hum. Evol*. **33**, 611-620 (1997).

117. M. J. Walker, M. López-Martínez, J. S. Carrión-García, T. Rodríguez-Estrella, M. San-Nicolás del-Toro, J.-L. Schwenninger, A. López-Jiménez, J. Ortega-Rodrigáñez, M. Haber-Uriarte, J.-L. Polo-Camacho, J. García-Torres, M. Campillo-Boj, A. Avilés-Fernández, W. Zack, Cueva Negra del Estrecho del Río Quípar (Murcia, Spain): a late Early Pleistocene hominin site with an 'Acheulo-Levalloiso-Mousteroid' Palaeolithic assemblage. *Quatern. Int.* **294**, 135-59 (2013).

118. A. López Jiménez, M. Haber Uriarte, M. López Martínez, M. J. Walker, Small-mammal indicators of biochronology at Cueva Negra del Estrecho del Río Quípar (Caravaca de la Cruz, Murcia, SE Spain). *Hist. Biol.* **32**, 18-33 (2018).

119. J. Vallverdú, P. Saladié, A. Rosas, R. Huguet, I. Cáceres, M. Mosquera, A. Garcia-Tabernero, A. Estalrrich, I. Lozano-Fernández, A. Pineda-Alcalá, Á. Carrancho, J. J. Villalaín, D. Bourlès, R. Braucher, A. Lebatard, J. Vilalta, M. Esteban-Nadal, M. L. Bennàsar, M. Bastir, L. López-Polín, A. Ollé, J. M. Vergés, S. Ros-Montoya, B. Martínez-Navarro, A. García, J. Martinell, I. Expósito, F. Burjachs, J. Agustí, E. Carbonell, Age and date for early arrival of the Acheulian in Europe (Barranc de la Boella, la Canonja, Spain). *PLoS One* **9**, e103634 (2014).

120. M. Arzarello, C. Peretto, Out of Africa: the first evidence of Italian peninsula occupation. *Quatern. Int.* **223-224**, 65-70 (2010).

121. G. Muttoni, G. Scardia, D. V. Kent, E. Morsiani, F. Tremolada, M. Cremaschi, C. Peretto, First dated human occupation of Italy at~ 0.85 Ma during the late Early Pleistocene climate transition. *Earth Planet. Sci. Lett*. **307**. 241-252 (2011).

122. M. Arzarello, C. Peretto, M.-H. Moncel, The Pirro Nord site (Apricena, Fg, Southern Italy) in the context of the first European peopling: Convergences and divergences. *Quatern. Int.* **389**, 255-263 (2015).

123. J. M. López-García, E. Luzi, C. Berto, C. Peretto, M. Arzarello, Chronological context of the first hominin occurrence in southern Europe: the Allophaiomys ruffoi (Arvicolinae, Rodentia, Mammalia) from Pirro 13 (Pirro Nord, Apulia, southwestern Italy). *Quatern. Sci. Rev*. **107**, 260-266 (2015).

124. J. Kappelman, M.C. Alçiçek, N. Kazancı, M. Schultz, M. Özkul, S. Sen, First *Homo erectus* from Turkey and implications for migrations into temperate Eurasia. *Am. J. Phys. Anthropol*. **135**, 110-116 (2008).

125. A. Vialet , G. Guipert, M. C. Alçiçek, *Homo erectus* found still further west: Reconstruction of the Kocabaş cranium (Denizli, Turkey). *C. R. Palevol.* **11**, 89-95 (2012).

126. A.-E. Lebatard, M. C. Alçiçek, P. Rochette, S. Khatib, A. Vialet, N. Boulbes, D. L. Bourlès, F. Demory, G. Guipert, S. Mayda, V. V. Titov, L. Vidal, H. de Lumley, Dating the Homo erectus bearing travertine from Kocabaş (Denizli, Turkey) at at least 1.1 Ma. *Earth Planet. Sci. Lett*. **390**, 8-18 (2014).

127. E. Güleç, T. White, S. Kuhn, I. Özer, M. Sağır, H. Yılmaz, F. C. Howell, The Lower Pleistocene lithic assemblage from Dursunlu (Konya), central Anatolia, Turkey. *Antiquity* **83**, 11-22 (2009).

128. H. Ron, N. Porat, A. Ronen, E. Tchernov, L.-K. Horwitz, Magnetostratigraphy of the Evron Member–Implications for the age of the Middle Acheulian site of Evron Quarry. *J. Hum. Evol*. **44**, 633-639 (2003).

129. A. Ronen, Quaternary sedimentology and prehistory on the Mediterranean coastal plain of Israel. *Quatern. Int*. **464**, 315-326 (2018).

130. M. Shemer, O. Crouvi, R. Shaar, Y. Ebert, A. Matmon, L. K. Horwitz, V. Eisenmann, Y. Enzel, O. Barzilai, Geochronology, paleogeography, and archaeology of the Acheulian locality of 'Evron Landfill in the western Galilee, Israel. *Quatern. Res.* **91**, 729-750 (2018).

131. O. Bar-Yosef, N. Goren-Inbar, *The Lithic Assemblages of 'Ubeidiya: A Lower Paleolithic Site in the Jordan Valley* (Hebrew Univ. of Jerusalem, 1993).

132. M. Belmaker, E. Tchernov, S. Condemi, O. Bar-Yosef, New evidence for hominid presence in the Lower Pleistocene of the Southern Levant. *J. Hum. Evol*. **43**, 43-56 (2002).

133. N. Goren-Inbar *et al*., Evidence of hominin control of fire at Gesher Benot Ya'aqov, Israel. *Science* **304**, 725-727 (2004).

134. C. S. Feibel, "Quaternary lake margins of the Levant Rift Valley" in *Human Paleoecology in the Levantine Corridor*, J. D. Speth, N. Goren-Inbar, Eds. (Oxbow Books, 2004), pp. 21-36.

135. G. Sharon, N. Alperson-Afil, N. Goren-Inbar, Cultural conservatism and variability in the Acheulian sequence of Gesher Benot Ya'aqov. *J. Hum. Evol*. **60** 387-397 (2011).

136. V. E. Shchelinsky *et al*., The Early Pleistocene site of Kermek in western Ciscaucasia (Southern Russia): stratigraphy, biotic record and lithic industry (preliminary results). *Quatern. Int.* **393**, 51-69 (2016).

137. V. E. Shchelinsky *et al*., Early Palaeolithic sites on the Taman Peninsula (Southern Azov Sea region, Russia): Bogatyri/Sinyaya Balka and Rodniki. *Quatern. Int.* **223-224**, 28-35 (2010).

138. T. Garcia, *et al*. Earliest human remains in Eurasia: New $^{40}Ar/^{39}Ar$ dating of the Dmanisi hominid-bearing levels, Georgia. *Quatern. Geochronol*. **5**, 443-451 (2010).

139. R. Ferring *et al*., Earliest human occupations at Dmanisi (Georgian Caucasus) dated to 1.85-1.78 Ma. *Proc. Natl Acad. Sci. U.S.A.* **108** 10432-10436 (2011).

Acknowledgments: We are grateful to M. Casado and Y. Gonzalez (IDAEA-CSIC) for their assistance in the analyses of the alkenones and J. Jadhav for preliminary analysis of Mediterranean climate variability in the CESM1.2 '2Ma' simulation. We thank H.-A. Blain for discussions and M. Irving for drafting fig. S1. The '2Ma' CESM1.2 simulations were conducted on the Institute for Basic Science (IBS) Center for Climate Physics (ICCP) supercomputer Aleph, a Cray XC50-LC system. Funding: We gratefully acknowledge financial support from the Leverhulme Trust grant RPG-2014-417 (P.C.T., V.M., and D.A.H.); the Catalan Government, Research Group 2021SGR00986 (J.O.G.); IBS, South Korea grant IBS-R028-D1 (A.T., K.-S.Y., and H.K.); the Human Origins Research Fund (C.B.S.); and the Calleva Foundation (C.B.S., S.A.P., and N.M.A.). Author contributions: P.C.T., V.M., and A.T. designed the study. V.M. and P.C.T. wrote the manuscript with contributions from A.T., S.A.P., N.M.A., C.B.S., P.L.G., and D.A.H. V.M., D.A.H, and J.O.G. undertook the pollen, foraminiferal isotope, and alkenone analyses, respectively. S.A.P., N.M.A., and C.B.S. developed the database for the early hominin sites for Europe and Southwest Asia. P.L.G. discussed the glacial geological record. A.T. developed and coded the two-dimensional climate envelope model and downscaled the

CESM1.2 data. K.-S.Y. conducted the CESM1.2 '2Ma' simulation and the MIS 34 freshwater perturbation experiments. H.K. conducted a series of isotopeenabled CESM1.2 freshwater perturbation simulations to estimate the overall amplitude of the freshwater forcing for the MIS 34 terminal stadial event. All authors contributed to the ideas in this paper. Competing interests: The authors declare that they have no competing interests. Data and materials availability: The paleoenvironmental data (*61*) reported in this manuscript are available through PANGAEA. The CESM1.2 climate model data from the MIS 34 water-hosing experiment (*62*) and the MATLAB model code for the habitat suitability model (*63*) used to generate Fig. 4 and figs. S4 and 5 are available on the ICCP data server. The previously published data from the CESM1.2 2Ma simulation are available on the OpenDAP and LAS server: https://climatedata.ibs.re.kr/data/hominin-habitats/2ma-transient-climate-simulation-data. The maps in Fig. 4 were generated with M_Map: a mapping package for MATLAB, version 1.4m, available at https://www.eoas.ubc.ca/~rich/map.html. The CESM1.2 code is available at https://www2.cesm.ucar.edu/models/cesm1.2/.

Supplementary Materials

Materials and Methods

Figs. S1 to S5

Tables S1

References (*64-139*)

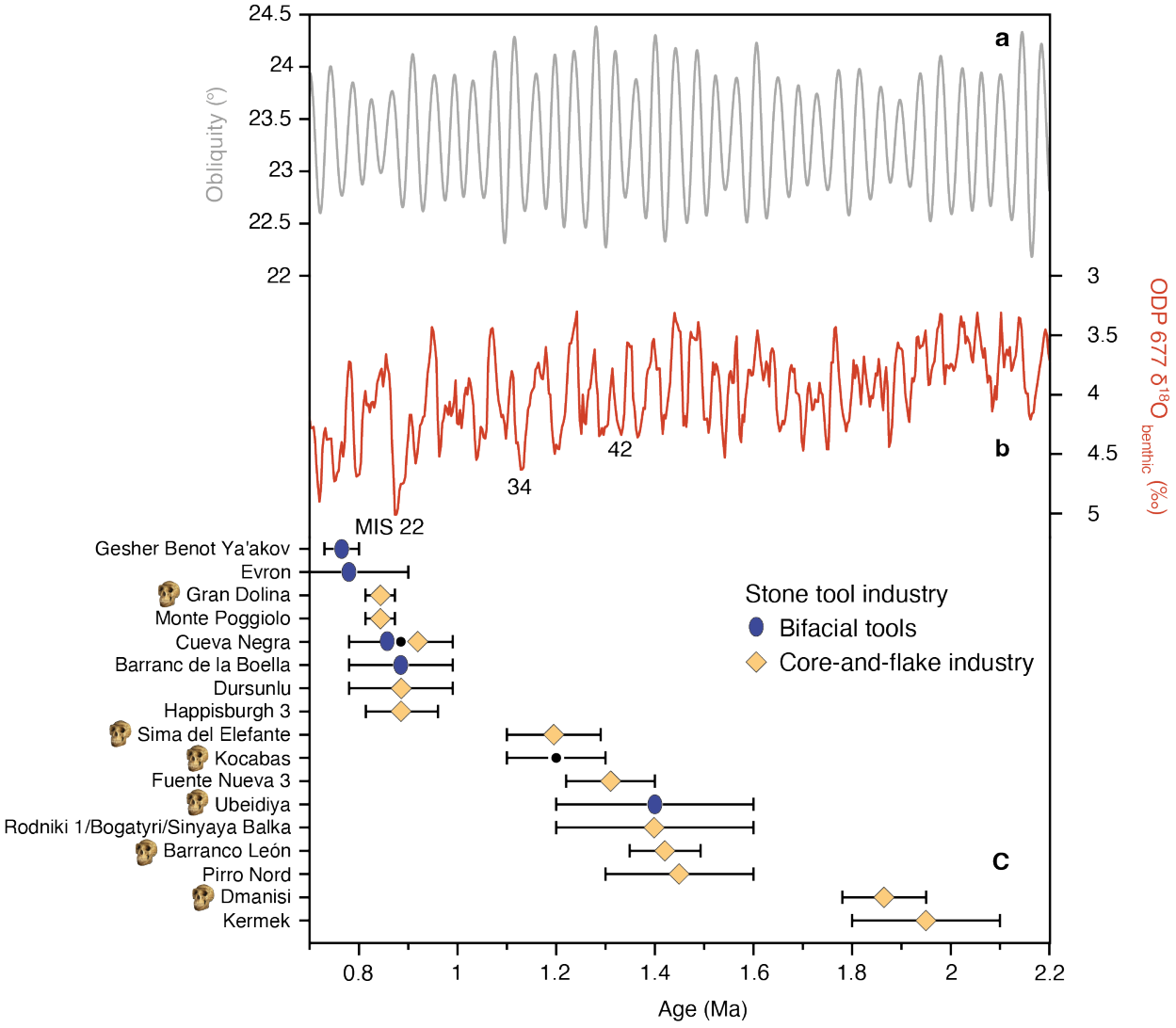

Fig. 1 Age estimates of European and SW Asian early hominin sites and paleoclimate context. **a,** Obliquity variations (*60).* **b,** benthic oxygen isotope record from Eastern Equatorial Pacific Site ODP677 (*15*). **c,** Age estimates of European and SW Asian early hominin sites (table S1). Stone tool industries are shown; sites with hominin remains are indicated by skull. Site selection is based on presence of human remains, strong evidence of humanly manufactured lithic artifacts and a secure chronological framework (*7*).

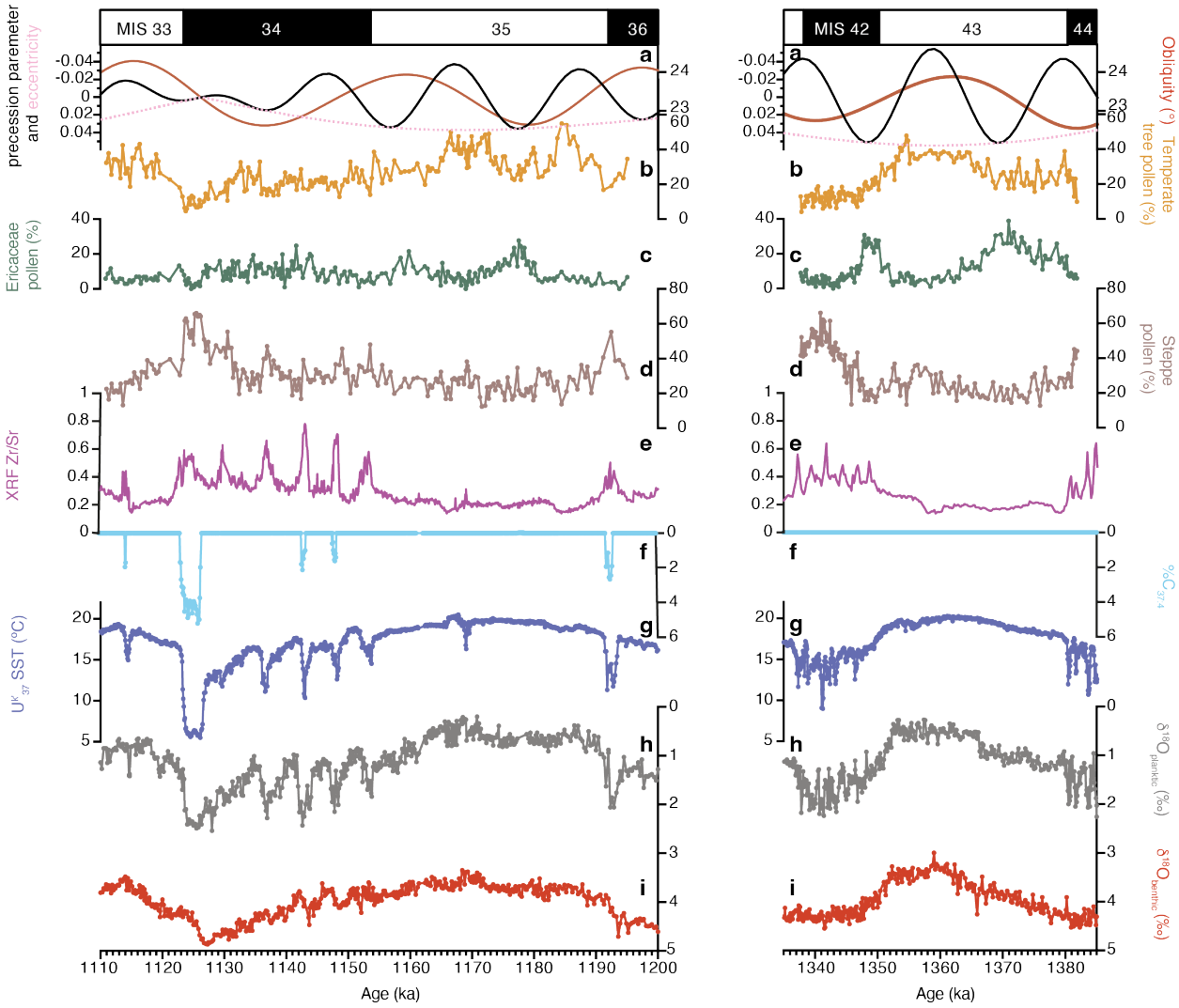

Fig. 2.2

Fig. 2.1

Fig. 2 U1385 paleoclimate records. The figure shows MIS 43 to 42 (right) and MIS 35 to 34 (left). **a,** Obliquity, eccentricity and precession parameter (*60*). **b,** Temperate (Mediterranean+Eurosiberian) tree pollen percentages. **c,** Ericaceae (heathland) pollen percentages. **d,** pollen percentages of steppe taxa (Poaceae, *Artemisia*, Amaranthaceae, *Ephedra*). **e,** XRF Zr/Sr ratio. **f,** abundance of tetra-unsaturated C37 alkenones (%$C_{37:4}$). **g,** alkenone-based $U^{k'}_{37}$ SST. **h**, planktic $\delta^{18}O$ of *Globigerina bulloides*. **i,** benthic $\delta^{18}O$ of *Cibicidioides* spp. Marine Isotope Stages (MISs) are indicated.

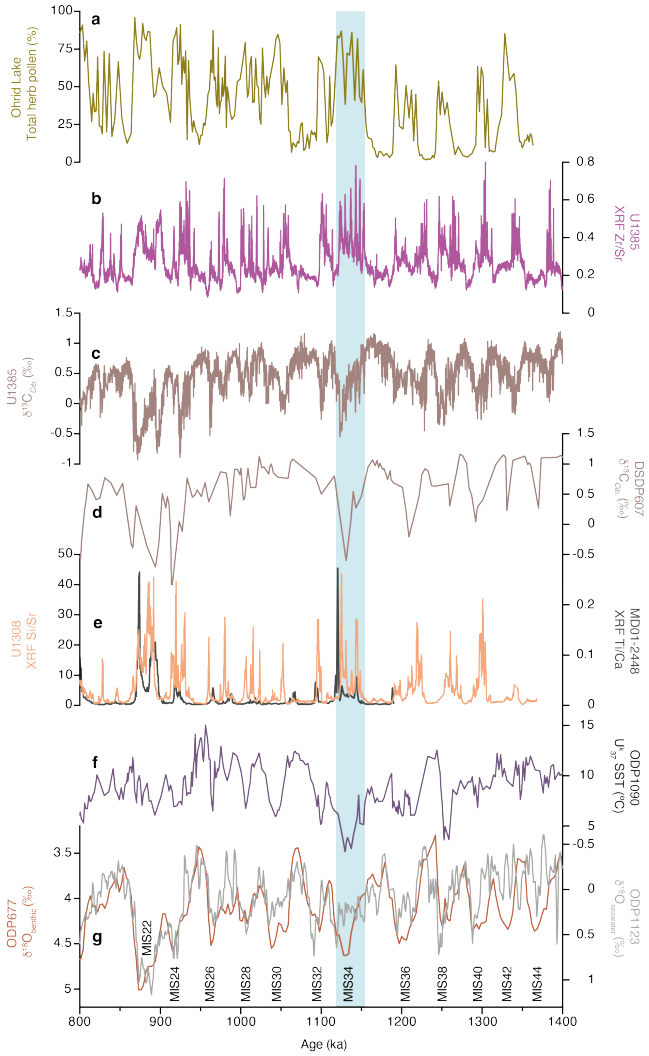

Fig. 3. Comparison of paleoclimate records over the interval 800 to 1400 ka. **a,** Lake Ohrid, (Albania - North Macedonia) total herb pollen percentages (*56*). **b,** U1385 Zr/Sr record (*28*). **c,** U1385 benthic $\delta^{13}C$ of *Cibicidioides* spp. (*28*). **d,** DSDP607 benthic $\delta^{13}C$ of *Cibicidioides* spp. from the North Atlantic (*54*). **e,** U1308 XRF Si/Sr ratio from the North Atlantic (*18*) and MD01-2448 XRF Ti/Ca ratio from the Bay of Biscay (*50*). **f,** ODP1090 alkenone-based U^{k}_{37} SST from the South Atlantic (*55*). **g,** ODP677 benthic foraminiferal $\delta^{18}O$ (orange) from the Eastern Equatorial Pacific (*15*) and ODP1123 deconvolved $\delta^{18}O$ composition of seawater (grey) from southwest Pacific (*16*). Marine Isotope Stages (MISs) are indicated.

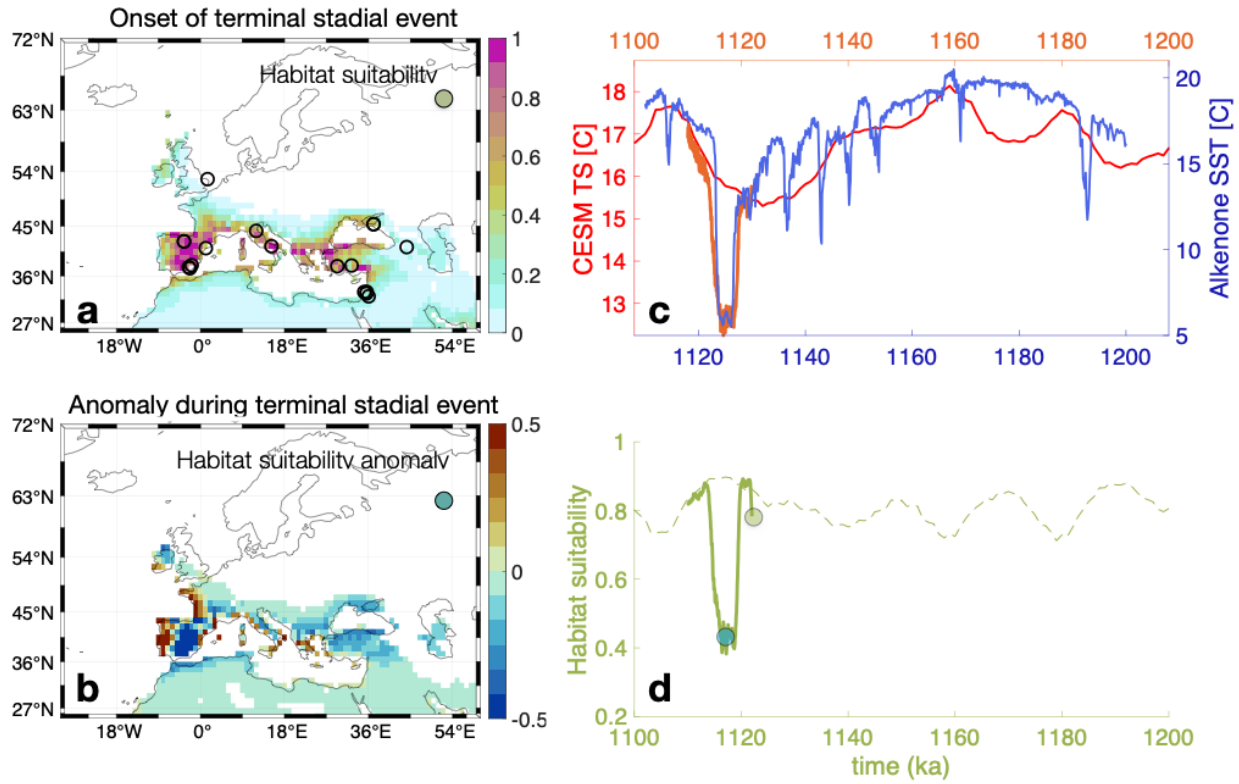

Fig. 4 MIS 34 terminal stadial event impact on early European human habitats. a, simulated habitat suitability (shaded) for the climate background conditions corresponding to the onset of the MIS 34 terminal stadial event conditions (1122 ka CESM1.2 initial conditions), along with locations (white circles) of hominin sites included in analysis discussed in text. Habitat suitability values smaller than 0.05 are not displayed. **b,** Anomaly of habitat suitability during the peak of the MIS 34 terminal stadial event [corresponding to model year 1117 ka (d)]. **c,** Western Iberian margin SST simulated by the '2Ma' transient CESM1.2 experiment (*34*) (red thin line) and by the freshwater perturbation experiment (thick carrot line) (*7*), and alkenone SST from U1385. The offset between the two timescale arises from differences between the U1385 age model (blue) (*7*) and the CESM1.2 age model (red), whose CO_2 forcing before 784 ka is

based on the model estimates of (*59*). **d,** simulated habitat suitability for '2Ma' (dashed) and for CESM1.2 MIS 34 terminal stadial event simulation (solid olive) for the western Iberian Peninsula (averaged over 4°W to 0°E, 38°N to 43°N). The timescale in olive corresponds to model age. The climate envelope model used in a,b,d is calculated using 17 early hominin sites (*7*) and 1000-year mean data of minimum annual temperature and calculated net primary productivity for these sites obtained from the '2Ma' simulation.

Science
AAAS

Supplementary Materials for

Extreme glacial implies discontinuity of early human occupation of Europe

Vasiliki Margari, David A. Hodell, Simon A. Parfitt, Nick M. Ashton, Joan O. Grimalt, Hyuna Kim, Kyung-Sook Yun, Philip L. Gibbard, Chris B. Stringer, Axel Timmermann, Polychronis C. Tzedakis

Correspondence to: p.c.tzedakis@ucl.ac.uk; axel@ibsclimate.org

This PDF file includes:

Materials and Methods
Figs. S1 to S5
Table S1

Materials and Methods

Integrated Ocean Drilling Program Site U1385

Materials

Site U1385 (37°34.285′ N, 10°7.562′ W, 2578 m below sea level) was drilled in December 2011 on the Promontório do Príncipe de Avis spur along the continental slope of the southwestern Portuguese Margin, SW of the Tagus river. Five holes were drilled, resulting in the recovery of a continuous 166.5-m sequence. A composite section was constructed by correlating elemental data measured by core scanning XRF at 1-cm resolution in all holes (*28, 64*). The U1385 record extends to 1.45 Ma (MIS47) with an average sedimentation rate of 11 cm kyr^{-1} (*28, 64*). Site U1385 is located very near the position of piston core MD01-2444 (37°33.68′ N, 10°08.53′ W, 2637 m below sea level; 27.45 m in length) and kasten core SHAK06-5K (37°34'N, 10°09'W; 2646 m below sea level; 3.44 m in length) and in the same region as piston core MD01-2443 (37°52.85'N, 10°10.57'W, 2925 m below sea level; length 29.48 m) (fig. S1). The composite southwestern Portuguese Margin climate record of the last 400 kyr in fig. S2 was constructed as follows: (i) planktic $\delta^{18}O$: MD01-2444 (0-194 ka) (*31, 65-67*) and MD01-2443 (194-400 ka) (*30*); (ii) alkenone sea surface temperature (SST): MD01-2444 (0-194 ka) (*38*) and MD01-2443 (194-400 ka) (*38*); (iii) pollen: SHAK06-5 (0-30 ka) (*65*), MD01-2444 (30-194 ka) (*31, 67, 69*) and MD01-2443 (194-400 ka) (*30*).

Foraminiferal isotope analyses

Oxygen and carbon isotope measurements of planktic and benthic foraminifera from Site U1385 were made at an average temporal resolution of ~200 years. The analytical methods are described in (*28, 64*). For planktic foraminifera, the surface-dwelling species *Globigerina bulloides* from the 250-350 μm size fraction was used. For benthic foraminifera, mostly *Cibicidoides wuellerstorfi* and occasionally other species of *Cibicidoides* from the >212 μm size fraction were used. In samples where specimens of *Cibicidoides* spp. were absent, the $\delta^{18}O$ of *Uvigerina peregrina* or *Globobulimina affinis* was used. All $\delta^{18}O$ values for each species were corrected to *Uvigerina* using the offsets +0.64 for *Cibicidoides* and -0.3 for *G. affinis* (*33*). For $\delta^{13}C$, only analyses of *C. wuellerstorfi* were used, whose epibenthic habitat records the $\delta^{13}C$ of dissolved inorganic carbon in deep water (*28*).

Alkenone SST

Samples for biomarker analysis (about 2.5 g sediment) were extracted with dichloromethane in an ultrasonic bath. Prior to extraction an internal standard of n-hexatriacontane and n-dotetracontane was added. The extracts were saponified with 10% KOH in methanol. The neutral lipid fraction was extracted with n-hexane which was concentrated under a gentle flow of nitrogen. After that, toluene was added and the solutions were derivatized with

bis(trimethylsilyl)trifluoroacetamide. The gas chromatography analysis for identification and quantification of (E,E)-15,22-heptatriacontadien-2-one [$C_{37:2}$], (E,E,E)-8,15,22-heptatriacontatrien-2-one [$C_{37:3}$] and (E,E,E,E)-8,15,22,29-heptatriacontanetetraen-2-one [$C_{37:4}$] was carried out on a Varian 3800 equipped with a CPSIL-5 CB column coated with 100% dimethylsiloxane (film thickness 0.12 mm) using hydrogen as carrier gas (50 cm/s). The samples were also analyzed by gas chromatography coupled to mass spectrometry (Thermo Trace GC Ultra-DSQ II) in electron impact ionization mode (70 eV) to discard coelutions that could deviate the measured ratios (*70*). The $U^{k'}_{37}$ index was calculated from the ratio of ([$C_{37:2}$]/([$C_{37:3}$] + [$C_{37:2}$]) (*71*). The values were converted into SST, using a calibration equation from sediment samples and annual average SST of overlying waters (*72*). Analytical errors were <10% and the uncertainty in the $U^{k'}_{37}$ determinations lower than 0.015 (ca ± 0.5 ºC) (*73*). The relative abundance of [$C_{37:4}$] was calculated as %[$C_{37:4}$] = 100·[$C_{37:4}$]/([$C_{37:4}$] + [$C_{37:3}$] + [$C_{37:2}$]). This ratio has been used to indicate the advection of low-salinity polar water masses to the Portuguese Margin (*37, 38*). According to (*74*), high %$C_{37:4}$ is an indicator of low sea surface salinity from polar water masses because it is synthesized in large amounts by Isochrysidales algae that occur widely in sea ice.

Pollen analysis

Sediment samples of 1.5-4 cm^3 were prepared for pollen analysis using the standard hot acid digestion technique. Fine sieving, through a mesh of 10 μm or less, was not used as it can result in a loss of pollen. Residues were mounted in silicone oil for microscopic analysis at magnifications of 400, 630 and 1000 times. Abundances are expressed as percentages of the main sum, which includes all pollen except *Pinus*, Pteridophyte spores and aquatics. *Pinus* was excluded from the main sum, as it is over-represented in marine sediments (*75*). A minimum of 100 pollen grains, excluding *Pinus*, spores and aquatics, was counted in each sample. Pollen studies from continental shelf sequences suggest that transport to these areas is controlled primarily by fluvial and secondarily by aeolian processes (*76*). Studies on modern pollen deposition in fluvial systems indicate the rapid incorporation of pollen to marine sediments (*76*). On the Portuguese Margin, aeolian pollen transport is limited by the direction of the prevailing offshore winds and pollen is mainly transported to the abyssal site by the sediments carried by the Tagus River (*77*). Comparison of modern marine and terrestrial samples along western Iberia has shown that the marine pollen assemblages provide an integrated picture of the regional vegetation of the adjacent continent (*77, 78*).

X-ray fluorescence (XRF) Analysis

Core scanning XRF measurements were made every 1 cm in all holes drilled at Site U1385 using an Avaatech XRF core scanner (*28, 66*).

Age model

For the 800-1450 ka section of U1385, Hodell and colleagues (*28*) have provided two timescales: (i) a revised LR04 chronology (*79*) based on correlation to the benthic $\delta^{18}O$ record of the Prob Stack (*80*); and (ii) an astronomically-tuned age model. Here, we used the latter developed by correlating sediment lightness (L*) at Site U1385 to the Mediterranean sapropel stratigraphy (*81, 82*), and to precession minima assuming a 3-kyr lag (*19*). It is worth noting that the relative phasing of our proxies within the same sediment sequence can be determined stratigraphically and is independent of the age model.

Selection of early Homo occupation sites

There has been long debate about whether some of the earliest European lithic assemblages are natural or anthropogenic, where taphonomic processes have been argued to be responsible for their creation, particularly where raw materials such as knapped quartz display few signs of conchoidal fracture (*83-87*). Here (table S1), we have taken a critical approach as advocated by Roebroeks and colleagues (*87*) and only included archeological sites where the published data provide strong evidence of humanly manufactured lithic artefacts and where taphonomic processes are an unlikely agency for their creation. Although this is inevitably a subjective approach, improved publication of the lithic evidence would allow re-assessment of assemblages, particularly if data on objective knapping attributes are included such as those suggested in (*88*). A secure chronological framework was also required for inclusion in the database.

Modelling

Community Earth System Model version 1.2 (CESM1.2) simulation covering last 2 Ma

To calculate orbital and millennial-scale changes in habitat suitability we used a simulation (*34*) conducted with the CESM1.2 in 3.75°×3.75° horizontal resolution, which covers the climate history of the past 2 Myr ('2Ma' simulation). Different transient interglacial-glacial segments were run in parallel and with an orbital acceleration of 5 and combined subsequently as a continuous climate trajectory, following the method presented in (*89*). The climate model uses orbital forcing (*90*) and previous estimates of the ice-sheet and greenhouse gas evolution throughout the Pleistocene from a modelling study (*59*). The realism of the '2Ma' simulation against paleoclimate data has been documented recently (*34*).

CESM1.2 MIS34 freshwater perturbation simulation

The MIS34 water hosing simulation is conducted with the CESM1.2 climate model, using time-evolving boundary conditions (greenhouse gases, Northern Hemisphere ice sheets, orbital forcing) from 1.122 to 1.110 Ma. The simulation uses orbital acceleration factor of 5 (except for the freshwater perturbation), as in the previous '2Ma' transient run. The transient freshwater

forcing is applied in the northern North Atlantic (50°N-70°N) with a peak value of 0.25 Sv at 1.117 Ma and a time evolution that mimics the U1385 Alkenone SST time series. The total freshwater amount added into the global ocean corresponds to ~23 m sea-level equivalent.

Climate envelope model

The climate envelope model used in this study is a statistical model, which computes the habitat suitability for early European hominins as a cumulative probability with respect to the Mahalanobis distance between any given duplet of climate input variables (minimum annual temperature [TS_{min}] and diagnosed net primary productivity [NPP]) and the same climate duplet variables obtained for the hominin sites at ages. More specifically, the climate envelope model is derived by extracting TS_{min} and diagnosed NPP (*91, 92*) from the CESM1.2 '2Ma' simulation downscaled onto a 1°x1° horizontal resolution mesh, for the locations and time periods corresponding to the early hominin sites (table S1) and constrained to be younger than 2 Ma. In cases where paleoenvironmental reconstructions indicate an interglacial context (table S1), climate data were extracted from the CESM1.2 '2Ma' simulation only for the age ranges corresponding to interglacial marine isotopic stages. Age uncertainties of the hominin sites are treated as individual data points on a 1000-year time mesh (fig. S4). Given the limited amount of independent archeological and fossil data (17 sites), we decided to derive a 2-dimensional climate envelope model, in contrast to previous studies which used 4-dimensional climate input manifolds (*34, 93*). This allows for a more robust estimation of a Mahalanobis distance model (*94-97*). The calculated probability distribution derived from the fossil site information (table S1) shows optimal climate conditions for a NPP of ~300 gC/m^2/year, which corresponds to previous estimates (*34, 98*), and for TS_{min} of about 5°C. The climate envelope model is further forced with the TS_{min} and NPP changes obtained from the freshwater perturbation experiment to determine the effect of the terminal stadial event on human habitat suitability (Fig. 4, fig. S5).

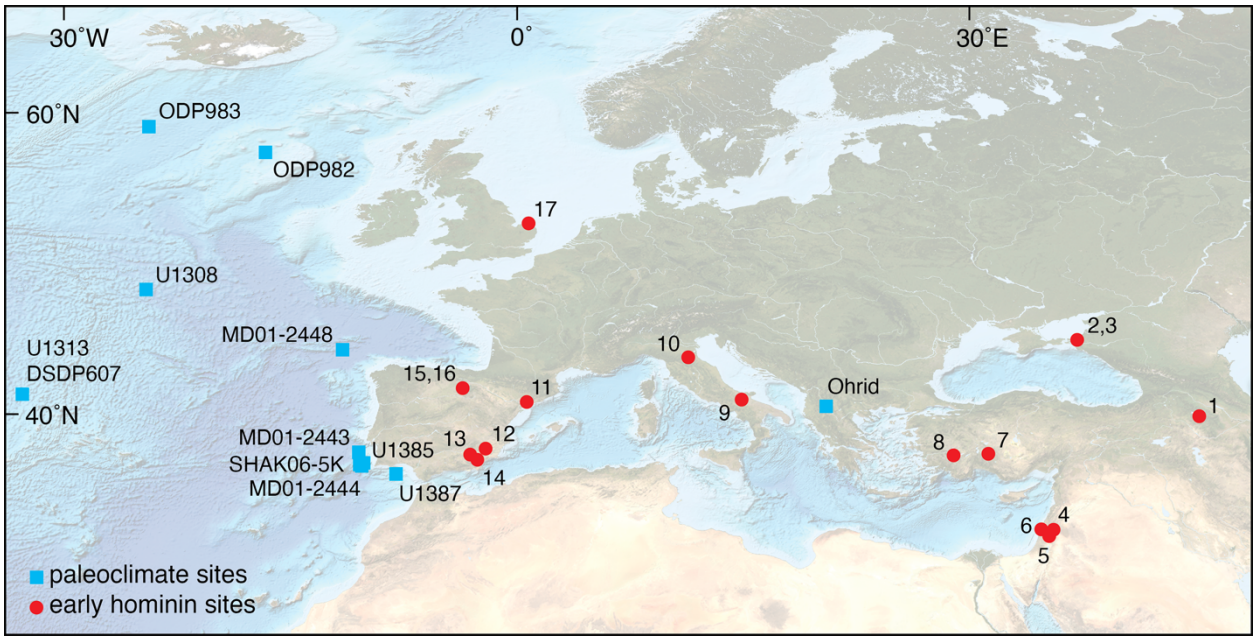

fig. S1.

Location of sites discussed in the main and supplementary text. Squares denote paleoclimate sites, dots early hominin sites: (1) Dmanisi, Georgia; (2) Rodniki 1 /Bogatyri/Sinyaya Balka, Russia; (3) Kermek, Russia; (4) Gesher Benot Ya'akov, Israel; (5) Ubeidiya, Israel; (6) Evron, Israel; (7) Dursunlu, Turkey; (8) Kocabaş, Turkey; (9) Pirro Nord, Italy; (10) Monte Poggiolo, Italy; (11) Barranc de la Boella, Spain; (12) Cueva Negra del Estrecho del Río Quípar, Spain; (13) Fuente Nueva 3, Guadix-Baza Basin, Spain; (14) Barranco León, Guadix-Baza Basin, Spain; (15) Sima del Elefante, Sierra de Atapuerca, Spain; (16) Gran Dolina, Sierra de Atapuerca, Spain; (17) Happisburgh 3, England.

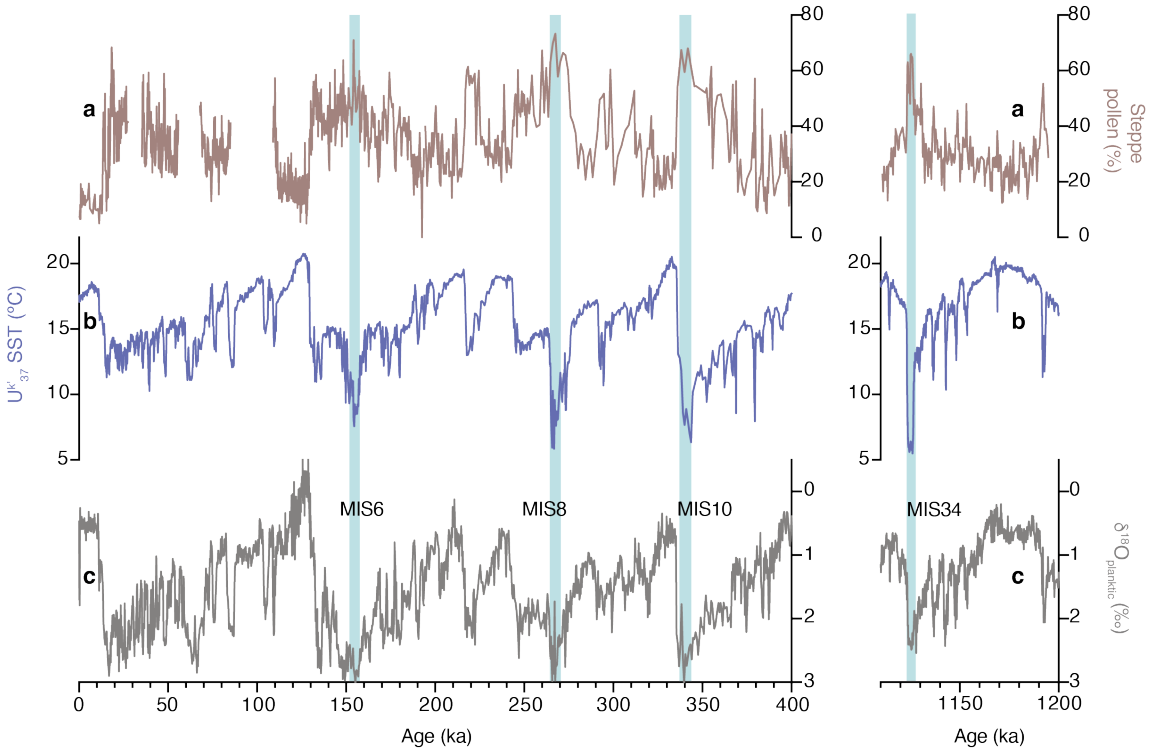

fig. S2.

Comparison of amplitude of cold and dry events during MIS 34 in U1385 and during the last 400 kyr in a composite record of southwestern Portuguese Margin sediment cores MD01-2444, MD01-2443 and SHAK06-5K. **a,** pollen percentages of steppe taxa (Poaceae, *Artemisia*, Amaranthaceae, *Ephedra*) (*30-31, 67-69*). **b,** Alkenone-based $U^{k'}_{37}$ SST (*38*). **c**, planktic $\delta^{18}O$ of *G. bulloides* (*30-31, 65-67*). Bars indicate the most extreme events.

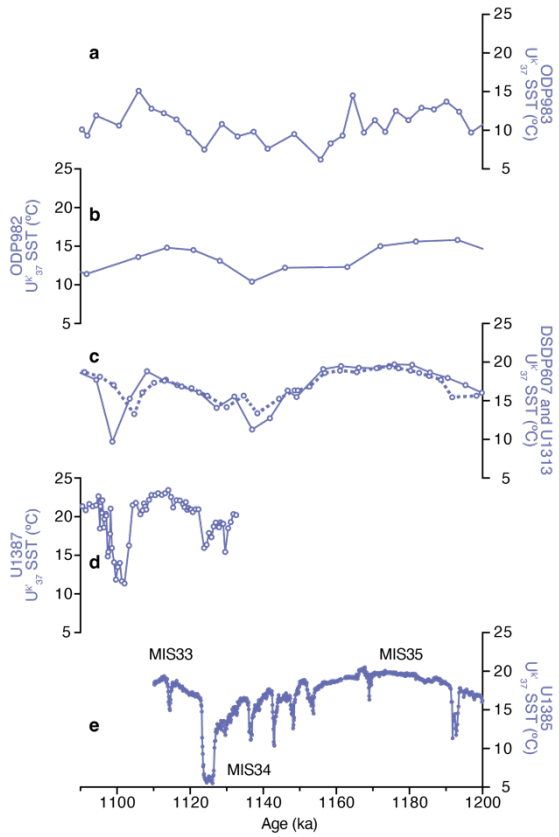

fig. S3.

North Atlantic $U^{k'}_{37}$ SST records. **a**, ODP983 (*99*). **b**, ODP982 (*100*). **c**, DSDP607 (dotted line) (*101*); U1313 (reoccupation of DSDP607; continuous line) (*102*). **d**, U1387 (*103*). **e**, U1385 (this study). Records are plotted on their own timescales, except U1387 which was shifted by 4 kyr to align with that of U1385.

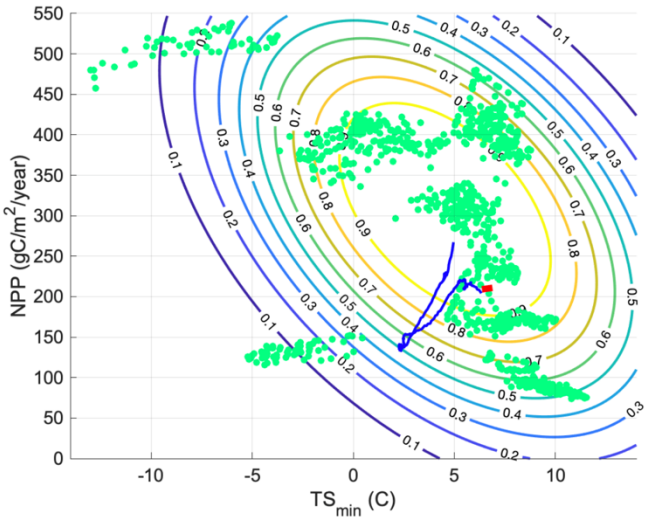

fig. S4.

Illustration of 2-dimensional climate envelope model. The green dots represent duplets of minimum annual air temperature (TS_{min}) and net primary productivity (NPP) obtained from the CESM1.2 '2Ma' for the 17 hominin sites under consideration of the dating uncertainties in 1000-year intervals. Contour lines correspond to the cumulative probability distribution (interpreted as habitat suitability) estimated from the inverse chi-squared distribution of Mahalanobis distances between climate state and the centroid defined by the hominin sites. The Mahalanobis distance calculation (*95*) also accounts for the 2-dimensional inverse co-variance matrix of the input data. The MIS34 terminal stadial event climate trajectory for a point on the Iberian peninsula (3°W, 42°N) is indicated for illustration (starting point 1122 ka marked as red dot).

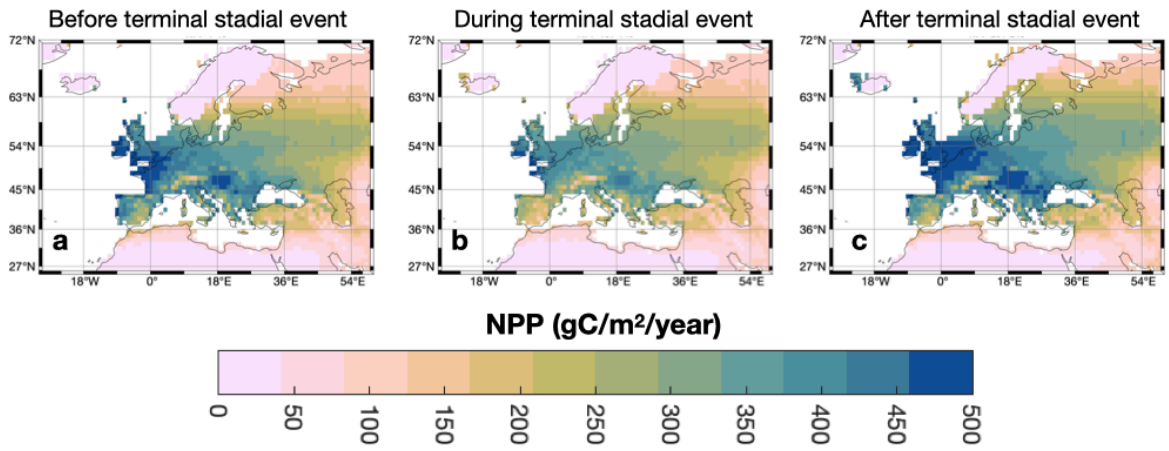

fig. S5.

Simulated Net Primary Productivity (gC/m^2/year) before, during and after the terminal stadial event.

table S1.
European and SW Asian early hominin sites. Criteria for the selection of sites are provided under Materials and Methods. Sites are ordered from NW Europe to SW Asia.

Site name*	Longitude (°)	Latitude (°)	Evidence for human occupation	Estimated Minimum Age (ka)	Estimated Maximum Age (ka)	Context†
Happisburgh 3, England (*104-105*)	1.53	52.83	Hillhouse Formation: cores, flakes; human footprints	814	960	Interglacial (*104*) 814-872 ka MIS21 936-960 ka MIS25
Gran Dolina, Sierra de Atapuerca, Spain (*106-107*)	-3.52	42.35	TD6.2: *H. antecessor*, cores, flakes TD4: cores, flakes	814	872	Interglacial (*108-109*) 814-872 ka MIS21
Sima del Elefante, Sierra de Atapuerca, Spain (*1-2, 110-111*)	-3.52	42.35	TE9: human mandible and phalanx; cores, flakes; cut-marked bones	1100	1290	Interglacial (*22,111*) (pre-Jaramillo) 1100-1097 ka MIS31 1110-1123 ka MIS33 1154-1192 ka MIS35 1232-1245 ka MIS37 1264-1290 ka MIS39
Barranco León, Guadix-Baza Basin, Spain (*3-4, 23, 112-113*)	-2.25	37.45	BL-D: deciduous molar; cores, flakes; butchered bone	1350	1493	Interglacial (*23, 114-115)* 1350-1380 ka MIS43 1390-1412 ka MIS45 1428-1452 ka MIS47 1470-1493 ka MIS49
Fuente Nueva 3, Guadix-Baza Basin, Spain (*3, 23, 112-113, 116*)	-2.50	37.70	FN3, levels 2 and 5: cores, flakes; butchered bone	1220	1400	Ambiguous (*23, 25*)
Cueva Negra del Estrecho del Río Quípar, Spain (*117, 118*)	-1.88	38.03	Units II-VI: cores, flakes; biface in Unit II	780	990	
Barranc de la Boella, Spain (*119*)	1.16	41.13	Unit II: bifacial tools	780	990	
Monte Poggiolo, Italy (*120-121*)	11.95	44.20	Level IMO1: cores, flakes	814	872	
Pirro Nord, Italy (*122-123*)	15.23	41.48	Level 10,13: cores, flakes	1300	1600	
Kocabaş, Turkey (*124-126*)	29.33	37.86	Level UT: fragmentary skull	1100	1300	
Dursunlu, Turkey (*127*)	32.39	37.97	Upper lignite: core, flakes	780	990	
Evron, Israel (*128-130*)	35.10	32.99	Clay layer: bifaces, cores, flakes	660	900	
Ubeidiya, Israel (*131-132*)	35.56	32.69	F1 Cycle: human teeth; bifaces, choppers, cores, flakes	1200	1600	
Gesher Benot Ya'akov, Israel (*133-135*)	35.62	33.01	Levels II, I and V: cleavers, bifaces, cores, flakes	730	800	

Kermek, Russia (*136*)	37.10	45.36	Bed 5: choppers, cores, flakes	1800	2100	
Rodniki 1 /Bogatyri/Sinyaya Balka, Russia (*137*)	37.11	45.36	choppers, cores, flakes	1200	1600	
Dmanisi, Georgia (*6, 138-139*)	44.20	41.33	Stratum B: human skulls and postcranial bones; cores, flakes	1780	1950	

† Based on paleoenvironmental reconstructions in indicated references.